NASA Technical Memorandum 104804

Block Distributions on the Lunar Surface: A Comparison Between Measurements Obtained from Surface and Orbital Photography

Mark J. Cintala and Kathleen M. McBride

October 1995

NASA Technical Memorandum 104804

Block Distributions on the Lunar Surface: A Comparison Between Measurements Obtained from Surface and Orbital Photography

Mark J. Cintala
Lyndon B. Johnson Space Center
Houston, Texas 77058

Kathleen M. McBride
Lockheed Engineering and Sciences Company
Houston, Texas 77058

October 1995

ACKNOWLEDGMENTS

This study was undertaken at the request of Ken Baker of the Automation, Robotics, and Simulation Division at the Johnson Space Center (JSC). Funding for the study was provided by JSC. High quality enlargements of the Lunar Orbiter photographs were printed by the JSC Metric Laboratory from negatives provided by the Lunar and Planetary Institute. Don Morrison reviewed an earlier version of this report--incorporation of his suggestions resulted in this much improved rendition.

This publication is available from the NASA Center for AeroSpace Information,
800 Elkridge Landing Road, Linthicum Heights, MD 21090-2934, (301) 621-0390.

ABSTRACT

Among the hazards that must be negotiated by lunar-landing spacecraft are blocks on the surface of the Moon. Unfortunately, few data exist that can be used to evaluate the threat posed by such blocks to landing spacecraft. Perhaps the best information is that obtained from Surveyor photographs, but those data do not extend to the dimensions of the large blocks that would pose the greatest hazard. Block distributions in the vicinities of the Surveyor I, III, VI, and VII sites have been determined from Lunar Orbiter photography and are presented here. Only large (i.e., $\gtrsim 2.5$ m) blocks are measurable in these pictures, resulting in a size gap between the Surveyor and Lunar Orbiter distributions. Nevertheless, the orbital data are self consistent, a claim supported by the similarity in behavior between the subsets of data from the Surveyor I, III, and VI sites, and by the good agreement in position (if not slopes) between the data obtained from Surveyor III photography and those derived from the Lunar Orbiter photographs. (The Surveyor III site is particularly suitable for this purpose because the blocks measured on both the Surveyor and Lunar Orbiter photography are confined to a well-defined crater.) Confidence in the results is also justified by the well-behaved distribution of large blocks at the Surveyor VII site.

Comparisons between the Surveyor distributions and those derived from the orbital photography permit these observations: (1) in all cases but Surveyor III, the density of large blocks is overestimated by extrapolation of the Surveyor-derived trends, (2) the slopes of the Surveyor-derived distributions are consistently lower than those determined for the large blocks, and (3) these apparent disagreements could be mitigated if the overall shapes of the cumulative lunar block populations were nonlinear, allowing for different slopes over different size intervals. The relatively large gaps between the Surveyor-derived and Orbiter-derived data sets, however, do not permit a determination of those shapes.

INTRODUCTION

Hazard assessment for lunar landings is a task of great importance, requiring painstaking and comprehensive analysis of the prospective landing sites. Such efforts often are impeded by the inadequate quality of data which does not allow the data to be analyzed to the desired level of detail. Principal among such detrimental factors are insufficient resolution of remote-sensing data and surface coverage that does not include the area of interest. Many of the requirements of such hazard assessments can be met only through extrapolations from low-resolution data to finer, more detailed scales, extrapolations from one area of the Moon to another, or both.

Among the quantifiable hazards faced by landing spacecraft are large blocks on the lunar surface. Not only could boulders cause instability problems during the touchdown phase of a landing, but they could also inflict critical damage to engine bells or other parts of the lander's undercarriage. Therefore, in evaluating and selecting a landing site, it is important to determine the size distribution of blocks on the surface as well as to assess their location. Most studies of block distributions on the Moon have been done with data returned by landed spacecraft, particularly by the Surveyor series of landers (e.g., Shoemaker et al., 1969; Shoemaker and Morris, 1970), although similar information obtained from Apollo surface photography has been used to estimate volumes of crater ejecta (e.g., Hodges et al., 1973; Muehlberger et al., 1972; Ulrich et al., 1975, 1981). Only a few studies have used orbital photography to measure block dimensions and distributions (e.g., Cameron and Coyle, 1971; Moore, 1971; Cintala et al., 1982; Lee et al., 1986). In a sense, however, these data are discontinuous because the landers provide high-resolution data over a limited area, while the orbital information extends over a wide region, but at much lower resolution.

Acquisition of additional data to support planning of piloted-lander missions undoubtedly would be expensive, and it is debatable as to whether the data provided by automated landers would be more or less useful in evaluating the boulder hazard than those obtained by orbiting precursors. It is therefore important to understand the limits to which each type of data can be used. The purpose of this contribution is to gauge the extent to which each of the two data types can be used to support the other. This will be done by comparing the block distributions obtained from the Surveyor I, III, VI, and VII spacecraft with those determined here from orbital photography of the region surrounding each of these four Surveyor landing sites.

A BRIEF OVERVIEW OF AVAILABLE PHOTOGRAPHY

Very high resolution orbital photography of the Moon (on the order of a meter resolution) exists in useful quantities, although its coverage of the planet is spotty at best. The best of these photographs are select Lunar Orbiter frames and the Apollo panoramic-camera products. Each has its advantages and disadvantages:

Apollo Panoramic Camera Photography—Each of the last three (J-Mission) Apollo Command/Service Modules included a Scientific Instrument Module, which contained mapping and panoramic cameras. Exposed at a nominal altitude of 111 km (60 nautical miles), features 1 to 2 meters across (9-18 μrad) can be resolved in photographs from the panoramic cameras. The nominal resolution holds only for the subspacecraft point since the high aspect ratio of the panoramic camera photographs results in oblique views of a large portion of each image. Because photography occurred in long sequences that often extended from terminator to terminator, variations in lighting can be extreme across the panoramic-camera collection.

High-Resolution Lunar Orbiter Photography—The Lunar Orbiter spacecraft (launched between 1966 and 1967) were equipped with motion-compensated medium-resolution (~165 μrad) and high-resolution cameras (~21.3 μrad). Thus, the high-resolution camera had a theoretical resolution of 1 meter from a 47-km altitude. Because most of the high-resolution photographs were intended to support Apollo site-certification activities or were made for purely scientific purposes, the lighting is generally optimal for interpretation of surface features. There are instances, however, when the terrain imposed severe lighting conditions on the automatic exposure system, resulting in local under- and overexposure. Brightly illuminated slopes near the lunar terminator represent such a case.

Lunar Orbiter photographs were used in this study of block distributions for three principal reasons: (1) most importantly, there is no Apollo panoramic coverage of any of the Surveyor landing sites, (2) the resolution and scale of the photography is such that the degree of photographic enlargement required for useful prints is lower than that necessary for comparable panoramic-camera photography, and (3) photography of the areas of interest was made under optimal illumination.

However, there are also some problems to be overcome in using Lunar Orbiter photographs. First, the design of the photographic system required that each photograph be assembled manually from individual 35-mm framelets. This process inevitably caused registration problems between framelets, resulting in a "venetian blind"

effect. Not only does this work against a visual impression of continuity, but small (and sometimes obvious) strips of the image are lost between framelets. Second, the bimat process used to develop the film on board the spacecraft (similar to the old Polaroid process) often left blemishes of varying size on the photographs, obscuring portions of the image. Third, the lunar control net during the time of the Lunar Orbiter missions was not well defined. The lunar coordinate system was not, therefore, as accurate as it has become with the use of Apollo data. Nevertheless, these few difficulties can be accommodated in most cases, and the Lunar Orbiter photographs remain a valuable resource—certainly the best for the purposes of this study.

THE SURVEYOR SITES

Five of the seven Surveyor spacecraft launched to the Moon landed safely. Except for Surveyor VII, all landed near the lunar equator, in the so-called "Apollo zone" (table 1). Their mission was to gauge the lunar surface in preparation for the early Apollo landings, which would take place near the lunar equator for safety reasons. Furthermore, the candidate Apollo sites were located in relatively smooth mare terrain to minimize potential topographic hazards. Surveyor I landed in south central Oceanus Procellarum, Surveyor III in extreme eastern Oceanus Procellarum, Surveyor V in Mare Tranquillitatis, and Surveyor VI in Sinus Medii (in the center of the Moon as seen from Earth). Surveyor VII, the only mission whose site was chosen purely on the basis of scientific interest, landed in the rugged ejecta deposits just to the north of the large, fresh crater Tycho. A malfunctioning vernier engine caused Surveyor II to enter an uncorrectable tumble and crash. Contact with Surveyor IV was lost about 2.5 minutes before touchdown, leading to speculation that its retrorocket exploded.

Table 1. Locations of Surveyor spacecraft on the Moon (ACIC coordinates, from Jaffe and Steinbacher, 1969). Negative latitudes are south of the equator.

Spacecraft	Date of Landing	Latitude	Longitude
Surveyor I	2 June 1966	-2.46	43.23° W
Surveyor III	20 April 1967	-2.99	23.34° W
Surveyor V*	11 September 1967	1.41° N (approx.)	23.18° E (approx.)
Surveyor VI	10 November 1967	0.51	1.39° W
Surveyor VII	10 January 1968	-40.88	11.47° W

* Surveyor V was not included in this study because of inadequate photographic coverage from orbit.

For the purposes of evaluating landing hazards, the block distributions of the mare sites are probably the most important to study because high-value landers will probably be targeted for mare (or very similar) areas. Each of the Surveyor sites in the maria (except for Surveyor V for which photographic coverage from orbit is inadequate for this

study) is treated below, but the Surveyor VII site is also included as a pathological case to demonstrate the wide range in block distributions that exist on the lunar surface.

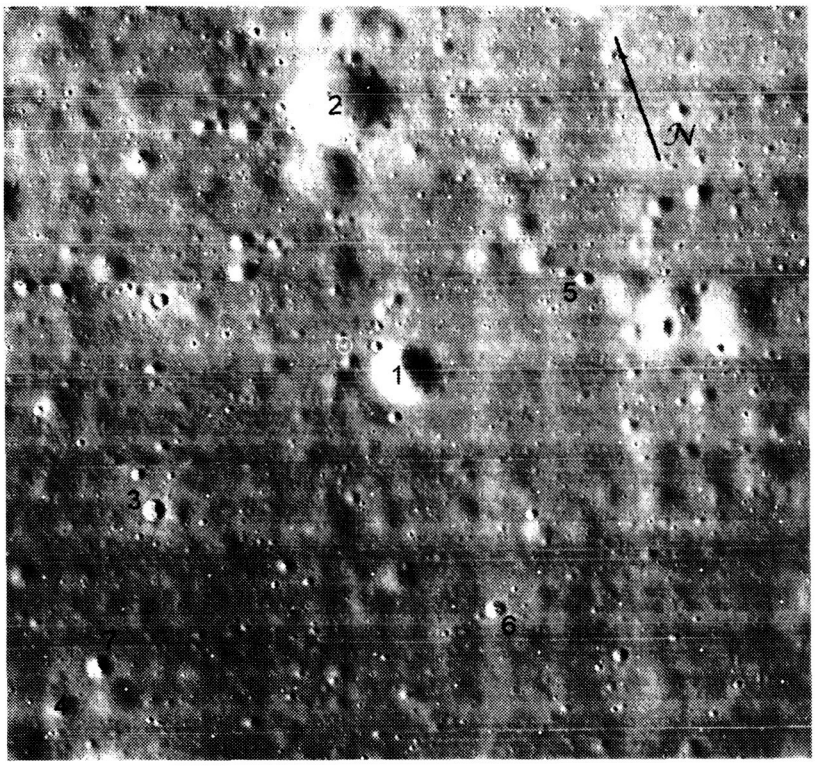

Figure 1. The Surveyor I area. All visible blocks in this and the subsequent three views were measured and catalogued. The numbers in this and the next three photographs indicate those craters listed in Appendix A. Crater 1 is about 180 m in diameter. The Surveyor 1 spacecraft is visible as a white dot in the small white circle near Crater 1. Part of Lunar Orbiter III photograph 183H$_1$.

Surveyor I

The Surveyor I spacecraft landed successfully in south central Oceanus Procellarum inside the broken rim of Flamsteed Crater on 2 June 1966. (The ACIC coordinates of this and the other four landed Surveyor spacecraft are listed in table 1.) The basalts in this area are some of the youngest on the Moon (between about 2.5 to 3.0 BY old as estimated on the basis of crater degradation; Boyce et al., 1974) and, as a result, they are covered by relatively thin regoliths (median depth of about 3.3 m; Oberbeck and Quaide, 1968). Of the four Surveyor sites studied here, this appears to be the smoothest (figure 1).

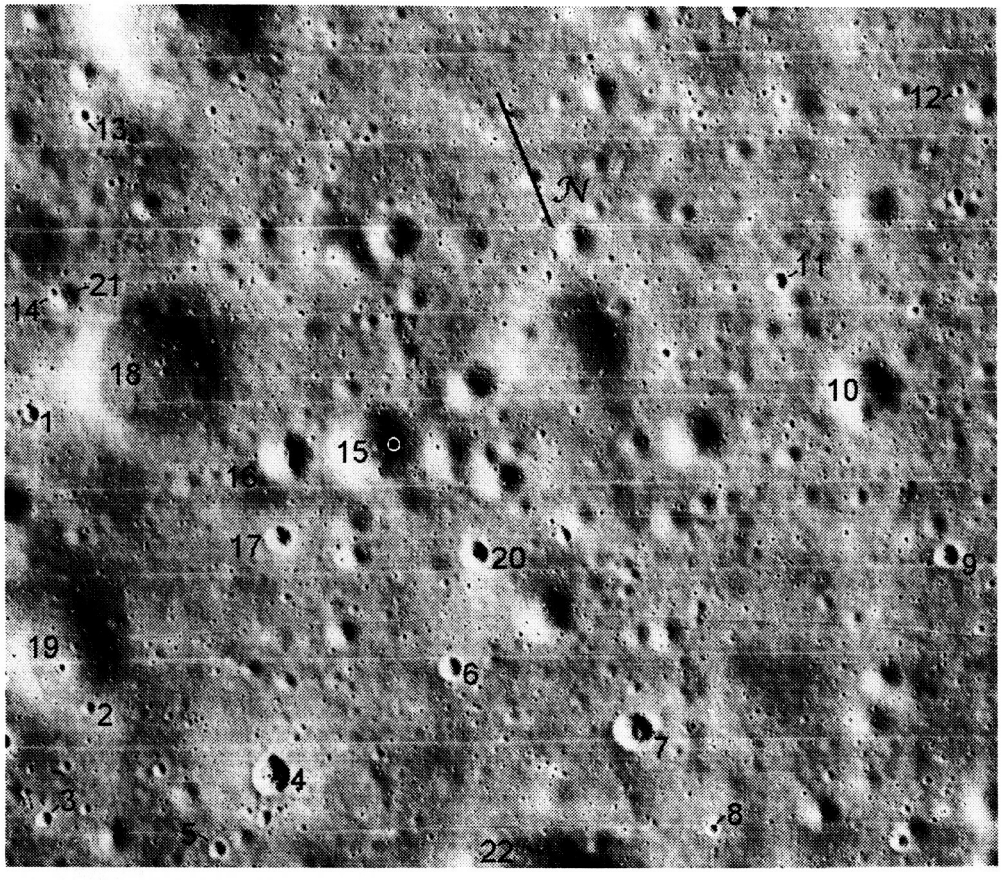

Figure 2. The Surveyor III area. All visible blocks in this view were measured and catalogued. The location of the Surveyor III spacecraft is indicated by the white circle inside Crater 15, which is about 240 m in diameter. Part of Lunar Orbiter III photograph 154H$_2$.

Surveyor III

Surveyor III landed in far eastern Oceanus Procellarum on 20 April 1967 and was followed by the Apollo 12 LM on 19 November 1969, which touched down less than 200 m from the Surveyor. The basalts at this site are somewhat older than at the Surveyor I locale (3.2 to 3.3 BY old [Papanastassiou and Wasserburg, 1971; Turner, 1971]), but are still considered to be relatively young in the scheme of lunar geology. Numerous secondary craters pepper this site, resulting in a somewhat more rugged terrain than the Surveyor I area (figure 2). Surveyor III actually landed inside an eroded crater with a diameter of about 240 m. Because the vernier engines did not shut down automatically, the spacecraft bounced a few times before coming to rest on the wall of the crater.

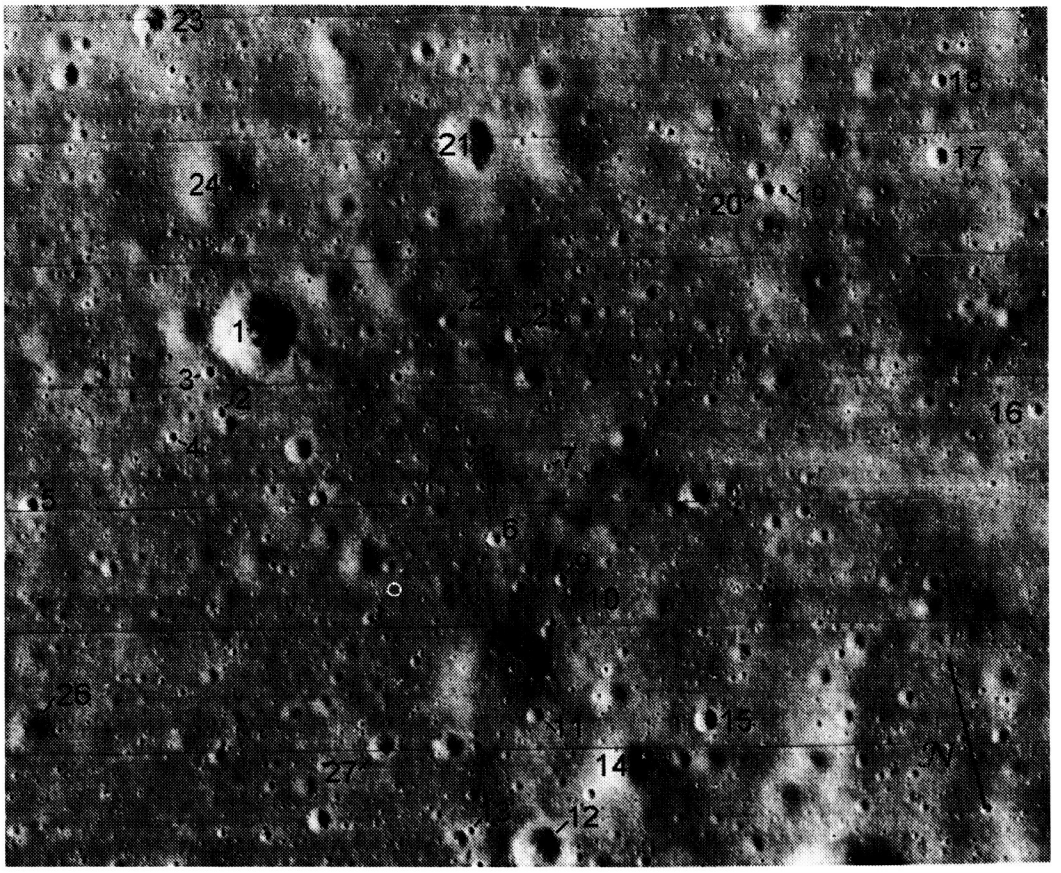

Figure 3. The Surveyor VI area. The location of the Surveyor VI spacecraft is indicated by the white circle just below and to the left of the center of the picture. Crater 21 is about 100 m in diameter.

Surveyor VI

Surveyor VI landed on 10 November 1967 just north and west of the center of the lunar nearside in Sinus Medii, the relatively small patch of mare that occupies the very center of the Moon's disk as seen from Earth. On the basis of crater degradation models, the basalts of Sinus Medii are roughly the same age as those at Surveyor III (Boyce et al., 1974). Even so, the Surveyor VI site appears to be somewhat less rugged than the Surveyor III area (figure 3), possibly because of the effects of secondary cratering at the latter site.

Surveyor VII

The last mission of the series had a distinctive scientific flavor, as Surveyor VII was targeted for one of the most rugged parts of the Moon exterior to a crater. The spacecraft touched down safely on 10 January 1968 on the ejecta deposits to the north of Tycho (figure 4), the freshest lunar crater of its size (about 85 km in diameter). The concept of "regolith thickness" begins to lose its meaning in the lunar highlands, which

are so pulverized from accumulated impacts that they have no bedrock layer for reference. When the chaotic deposits from a large crater are included, as in this case, the local definition of the regolith becomes more philosophical in nature. There are, however, many obvious deposits of impact melt (rock fused by the effects of the impact-generated shock) in the vicinity of Surveyor VII. If these deposits were treated by the same standards as mare basalts, they are so young (on the order of 100 MY; Arvidson et al., 1976; Neukum and König, 1976) as to possess regoliths only a few tens of centimeters thick.

Figure 4. The Surveyor VII area. The location of the Surveyor VII spacecraft is indicated by the circle; this view is about 10.5 km across. Note the ubiquitous pools and flows of impact melt. Part of Lunar Orbiter V photograph 128H$_2$.

DATA COLLECTION

Method—The block-size and distribution data used in this study were collected from enlarged prints of Lunar Orbiter frames with a CalComp 9500 series digitizing tablet. Points on each block were recorded as *x-y* coordinates. A series of programs, most of which were adapted from Grenander et al. (1976), reduced these *x-y* measurements to lunar latitudes and longitudes, which were converted, in turn, to the latitude and longitude of the block on the Moon as well as to its linear dimensions. Whenever

possible, each block was measured across its largest dimension in keeping with a conservative approach to an evaluation of blocks as possible hazards. The control net used in calculating the latitudes and longitudes was similar to that used to calculate the corner coordinates of the Lunar Orbiter photographs during their missions in the late 1960s. While this net is not as accurate as the Apollo-based system currently used for lunar cartography, it is self-consistent and yields good results for the purposes of this study.

Most blocks on existing lunar photographs are small features, and it is difficult to perform measurements near the limit of resolution of a photograph. The actual edges of the features being measured—the blocks in this case—are, more often than not, blurred and poorly defined. The advantages of enlarging the photograph are limited, as it is easier for the eye to work with a smaller image than with one that is enlarged too much. A balance had to be found, in this case, among the degree of photographic enlargement, the resolution of the digitizing tablet, and the size of the crosshairs on the cursor.

Table 2. Data for Lunar Orbiter photographs used in measuring block dimensions and locations. The *Resolution limit* is the theoretical resolution of the photographic system. The *"Line pair"* assumes that an actual feature could be discriminated from the background if it had a dimension 2.2 times the resolution limit. The *Enlargement scale* is the scale of the enlarged photograph used on the digitizing tablet, expressed here in meters on the lunar surface per millimeter on the photograph.

	Photograph number (LRC System)	***Spacecraft altitude (km)***	***Sun elevation (degrees)***	***Resolution limit (m)***	***"Line pair" (m)***	***Enlargement scale (m/mm)***
Surveyor I	LOIII $183H_1$	53.4	17.0	1.14	2.50	4.2
Surveyor III	LOIII $154H_2$	51.3	23.8	1.09	2.40	4.1
Surveyor VI	LOII $121H_3$	49.4	29.3	1.05	2.31	2.9
Surveyor VII	LOV $128H_2$	232.7	9.4	4.96	10.91	18.6

As an example, take the case of the Surveyor III photograph (table 2). The digitizing tablet has a nominal resolution of 0.025 mm, which, at the scale of the photograph used in this study, translates to about 10 tablet units per meter on the surface. Thus, the tablet's resolution was not a factor in introducing potential errors. Even with such good spatial resolution, however, the crosshairs on the tablet's cursor must be wide enough to minimize eyestrain on the part of the person doing the digitizing. In this particular case, the crosshairs are 0.13 mm across, which translates almost exactly to 5 tablet units. At the scale of the photograph, this corresponds to about 0.5 meters on the lunar surface. To minimize errors, the center of the crosshairs was not used to indicate each point. Instead, the corner defined by the edges of the crosshairs was used; this required that the orientation of the cursor relative to the *x-y* grid of the tablet remain as constant as possible for each of the points digitized on a given block. The relative errors incurred in measuring the blocks at the limits of a photograph's resolution are larger for the smaller

blocks. The result is sometimes a calculated block dimension that is clearly smaller than that actually visible on the photograph. Such cases occurred in this study for every Surveyor site, and those blocks were eliminated from consideration.

Finally, some blocks were missed because they were located in shadowed areas. When such regions were sufficiently large relative to the area of the photograph, their physical areas on the lunar surface were determined with a planimetric routine and subtracted from the area of the photograph. In the case of the orbital photography of the Surveyor VII site, sun-facing slopes were so overexposed that it was impossible to identify any features in those regions. These areas were also measured and subtracted from the total.

Statistics: Areal Frequency—To maintain compatibility with the measurements made from the photographs taken by the Surveyor spacecraft, the block distributions derived here from the Lunar Orbiter photography are presented as cumulative size-frequencies. In such a distribution, the number of blocks equal to or larger than the minimum dimension of each size bin is plotted against that minimum dimension (Shoemaker et al., 1969; Shoemaker and Morris, 1970). The error bars in the figures represent one standard deviation on the assumption that the block populations are Poisson distributed. Defining n_d as the number of blocks with a maximum dimension greater than d and A as the area over which those blocks were found, the areal density a_d is given by

$$\alpha_d = \frac{n_d}{A} \tag{1}$$

and the confidence interval σ_d is

$$\sigma_d = \frac{\alpha_d}{N^{1/2}} \tag{2}$$

More detailed discussions of the cumulative distribution as applied to crater counts can be found in (Crater Analysis Techniques Working Group, 1979). The data in numerical form are given in Appendix B.

Block Dimensions—As described above, it would be difficult to quantify the potential error associated with the measurement of block dimensions. Insofar as the accuracy of the digitizing tablet is significantly greater than the resolution limitations of the photography, it is likely that the most important source of error is in detecting the edges of the blocks. To minimize variations due to user bias, one of us (KMM) performed all of the data collection. Note that the data obtained for the block sample inside Surveyor Crater agreed well with those obtained from Surveyor III photography (figure 14). This is the best site for such a comparison because the Surveyor III data were obtained from blocks within Surveyor Crater. This, in turn, provided a well-delineated area to assess on the orbital photograph. The agreement between the two measurement techniques lends support, albeit qualitative, to the accuracy of the data obtained from the Lunar Orbiter photography.

Data Subsets—The distributions for the Surveyor I, III, and VI sites are presented as three distinct groups: *blocks inside craters*, *blocks between craters* (intercrater), and *the sum of both* (all blocks). No such distinctions were made in the case of the Surveyor VII site since most of the craters there are small and filled with shadows as a result of the low illumination angle. In many instances, it was difficult to judge the location of the rim crest of a given crater—a block was considered to be inside a crater when its position was within 1.1 crater radii of that crater's estimated center. This arbitrary value not only removed the requirement of judging the relative locations of many blocks under extreme lighting conditions, but it also included most of the topography associated with the crater rim, which rightly should be considered as much of a hazard as the crater's interior. The calculation to determine the status of each block relative to the crater locations was performed subsequent to the digitizing process. The size of each crater with which blocks were associated and the location of its center were both determined. The location of each block was then calculated relative to the size and location of each such crater.

Resolution Considerations—Every photograph possesses a *resolution limit*, which is most often given as the size of a pixel (picture element) or as the width of a scan line. (In the case of photographic film, this limit is dependent on the optics of the photographic system and the grain of the film.) This value, however, is more useful as a description of the performance of the imaging system than it is in describing the photography itself. More useful, perhaps, is the *line pair limit*, which is the minimum size of an object that can be identified on the photograph. This limit is typically taken as 2.2 times the resolution limit (2.2 scan lines or 2.2 pixels) from which it gets its name.

THE DATA

The Surveyor I Site

The three block distributions at the Surveyor I site are displayed in figure 5. (Unless specified otherwise, the data in these figures are plotted in equal logarithmic intervals along the abscissa.) The relative positions of the three subsets are typical of these plots in that the density of blocks inside craters at the mare sites is significantly greater than that between craters. Since the density of all blocks is derived from those blocks inside and outside the craters, it always lies between the two end-members. Note that the distributions undergo a fairly rapid change in slope as smaller dimensions are approached. This is a consequence of a decrease in the number of blocks visible as the limit of resolution is approached, an effect common in similar plots of crater densities. Table 2 shows that the line-pair limit for blocks in the photograph of the Surveyor I site is about 2.5 m (table 2), corresponding to the dimension at which the loss of blocks becomes apparent in figure. 5. This effect occurs at each of the other three sites examined in this study. It must be emphasized that the apparent decrease in block densities at smaller sizes in figure 5 and in similar subsequent plots is an artifact of photographic resolution and does not represent a real drop-off in the areal density of blocks on the lunar surface.

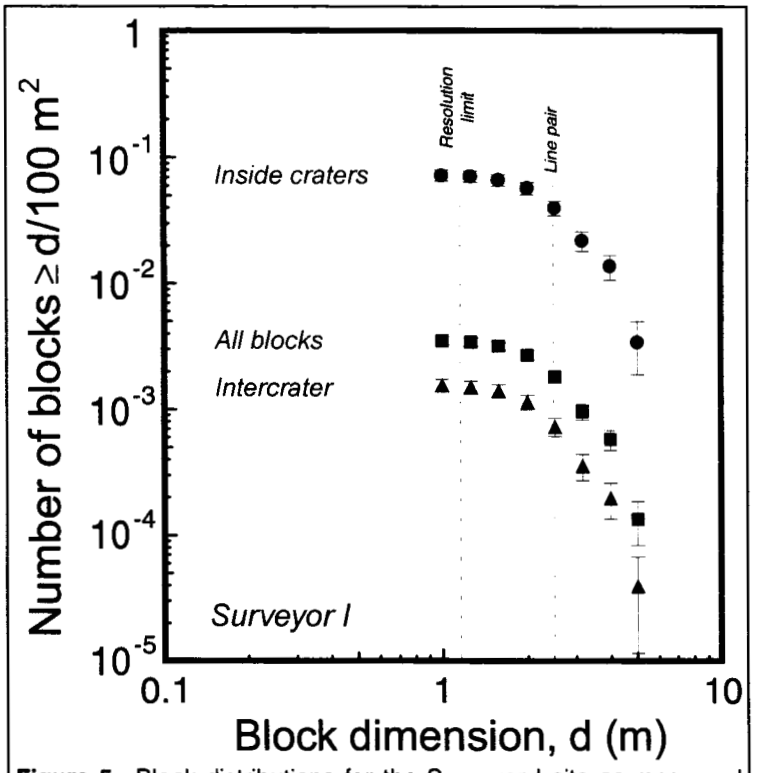

Figure 5. Block distributions for the Surveyor I site as measured from Lunar Orbiter photography. For illustrative purposes, points are plotted for sizes smaller than the line-pair limit of the photograph. Because the distributions begin to level off rapidly as that limit is approached, it is apparent that many smaller blocks were not measurable. This is also the case for the next three figures. The error bars in this and subsequent similar figures represent one standard deviation.

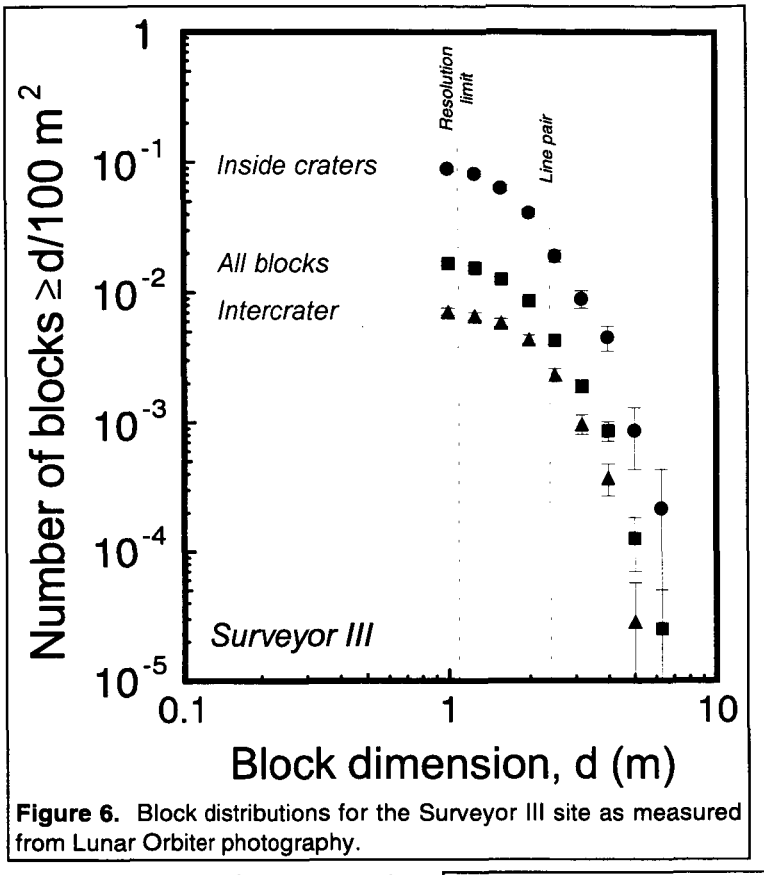

Figure 6. Block distributions for the Surveyor III site as measured from Lunar Orbiter photography.

The Surveyor III Site

The block distributions for the Surveyor III site are illustrated in figure 6, in which the relative positions of the block distributions at the Surveyor I site are mimicked. The block densities at the latter location, however, are uniformly greater than at the Surveyor III site, a difference that is probably related to the relative regolith thicknesses at the two sites. As craters on a mare surface accumulate, the thickness of the debris layer created by the impacts also increases. Consequently, larger impacts are required to penetrate this regolith layer if blocks are to be produced from the underlying basalts. Because the frequency of formation of craters drops with increasing crater size, the rate at which new blocks are created decreases with time (or increasing regolith thickness). This buffering effect will be addressed in more detail in a subsequent section.

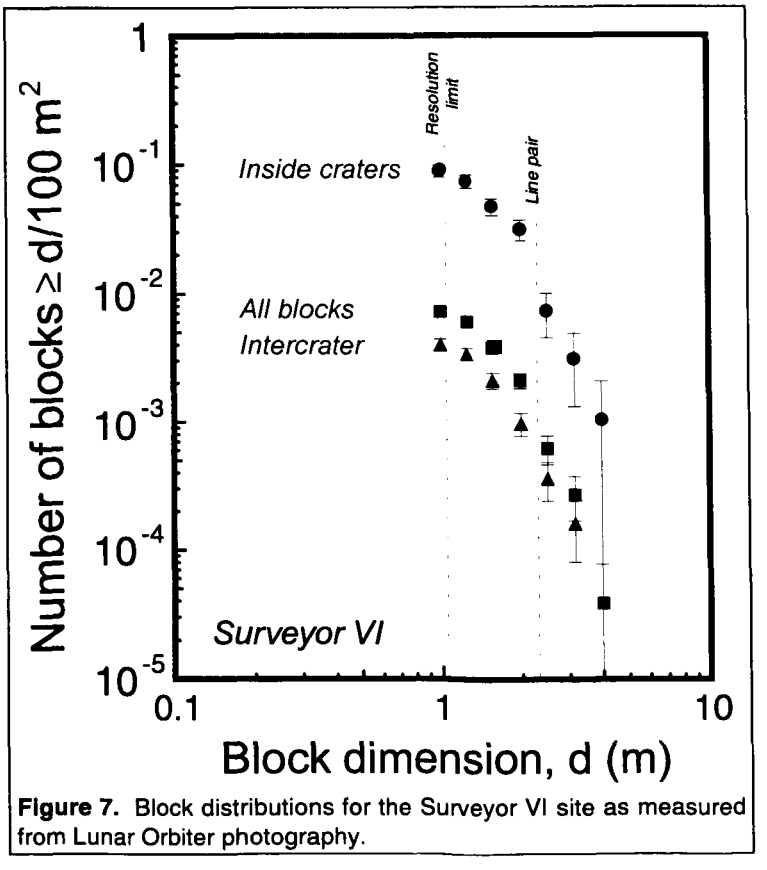

Figure 7. Block distributions for the Surveyor VI site as measured from Lunar Orbiter photography.

The Surveyor VI Site

The block distributions in the third mare site examined in

this study are presented in figure 7. The block densities at this location are unremarkable in light of those of the previous two sites.

The Surveyor VII Site

It is immediately obvious from the Lunar Orbiter photograph of the Surveyor VII locale that its block distribution is in a class different from that of the three mare sites, and the measurements confirm this impression (figure 8). Compared to the Surveyor I distributions, for instance, the density of all blocks 10 meters across or larger at the Surveyor VII site is a factor of 20 greater than the density of blocks inside craters at Surveyor I, and a factor of 2000 greater than the intercrater distribution at the latter site. Further comparisons are given below.

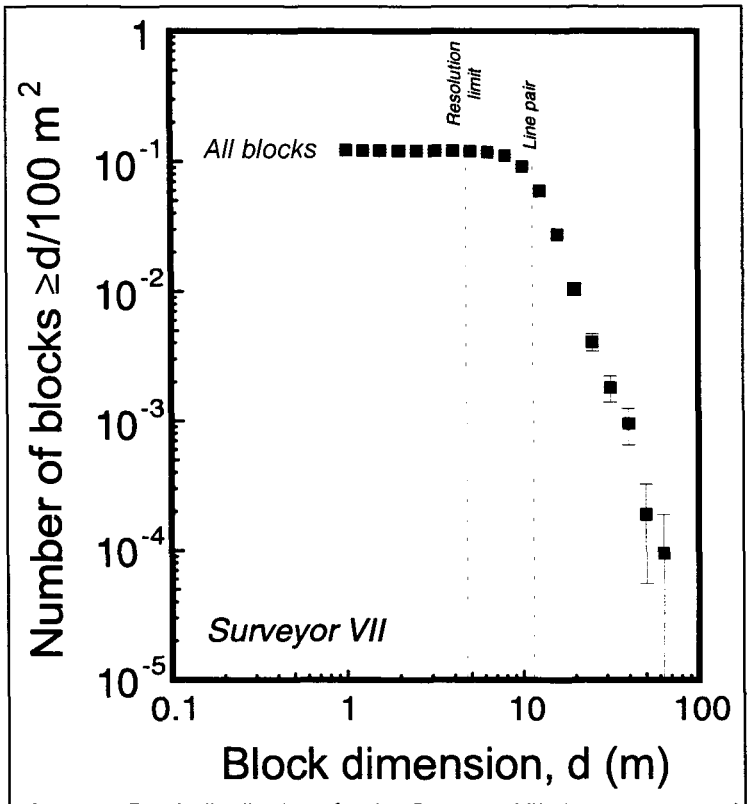

Figure 8. Block distributions for the Surveyor VII site as measured from Lunar Orbiter photography. Note the values on the axes of this figure as compared to those of the previous three. A breakdown of the block sample into inter- and intracrater distributions is not possible at this locale.

COMPARISONS OF THE FOUR SURVEYOR SITES

A comparison of the block distributions at the three Surveyor mare sites is hindered by the limiting resolution of the Lunar Orbiter photographic systems: blocks larger than about 2.5 m in dimension are simply few in number. As a consequence of the restricted number of data points, rigorous statistical comparisons are of limited usefulness. Nevertheless, some general information can be extracted from the data, and this section will make some comparisons between the sites.

It was shown in the previous section that the resolution limit of the Lunar Orbiter photographs is reflected in the data for the three mare sites at sizes near 2.5 meters; similar effects are visible in the Surveyor VII counts at dimensions of about 11 meters. Thus, to minimize spurious effects due to these resolution limitations, only blocks larger than the line-pair limits at their respective sites will be treated here. The data will be

considered in terms of the three subgroups discussed above: all blocks at each site, blocks inside craters, and intercrater blocks.

All Blocks

The four distributions for all blocks measured at the four sites are illustrated in figure 9. The extreme differences between the mare sites and the Surveyor VII locale are apparent, but the differences in block density among the three mare sites are much less obvious. Indeed, there is little basis to suggest that the Surveyor I and III sites are different, although the density at smaller sizes might be slightly lower at Surveyor I. While the Surveyor VI site is somewhat less populated than either of the other two mare sites, the general shape of the distribution appears to be similar to those of the other two, albeit on the basis of only three points.

A common feature of all four cases is the departure from a simple power-law distribution (which would appear as a straight line in such log-log plots). Each of the mare sites exhibits a change in slope at the larger end of its range, while the Surveyor VII distribution displays a noticeable variation at the larger sizes. Little more in terms of a quantitative description is warranted as the data are sparse and therefore provide few constraints on interpretations. Additionally, the shapes of the mare distributions at the smaller sizes are still consistent with a drop-off in block numbers due to limitations of photographic resolution, lending another potential complication. Nevertheless, the consistent nonlinear behavior of the four distributions cautions against overinterpretation of simple power-law fits to the data.

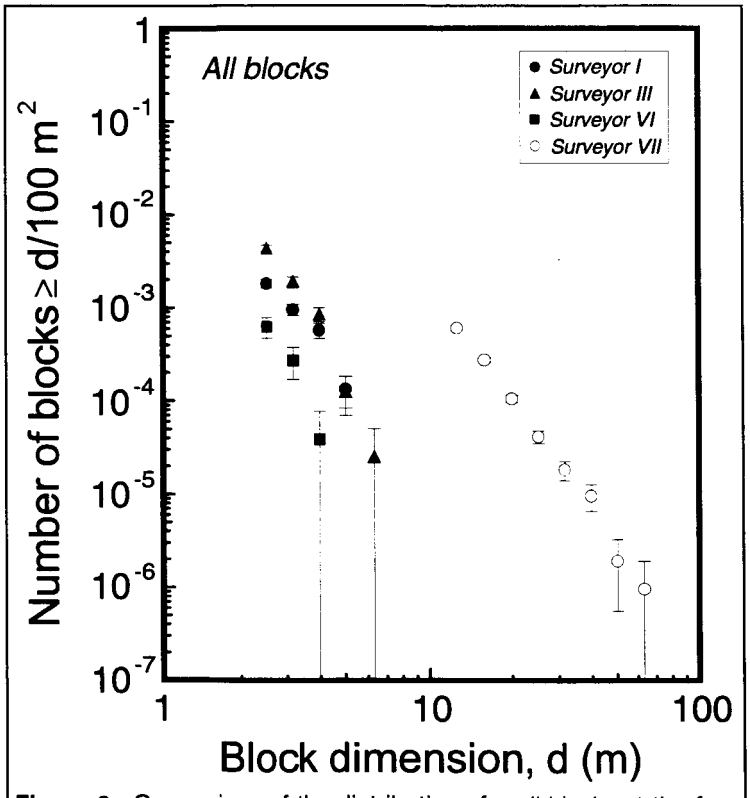

Figure 9. Comparison of the distributions for all blocks at the four Surveyor sites studied here. Only those blocks above the "line-pair" limit are used in this and the next two figures.

Blocks Inside Craters

The distributions of blocks inside craters at the three mare sites are illustrated in figure 10. The unique nature of the Surveyor VII site with respect to this study precludes any subdivision of its block population into this category. A reversal of the Surveyor I and III distributions occurs in this figure relative to those in figure 9 in that the density inside craters at the Surveyor I site is somewhat higher than at the Surveyor III locale. These two trends again exhibit excursions from linearity; the Surveyor VI data are much closer to a simple power-law in form, but the limited number of data points and the relatively large uncertainties on the existing points do not encourage a more forceful statement.

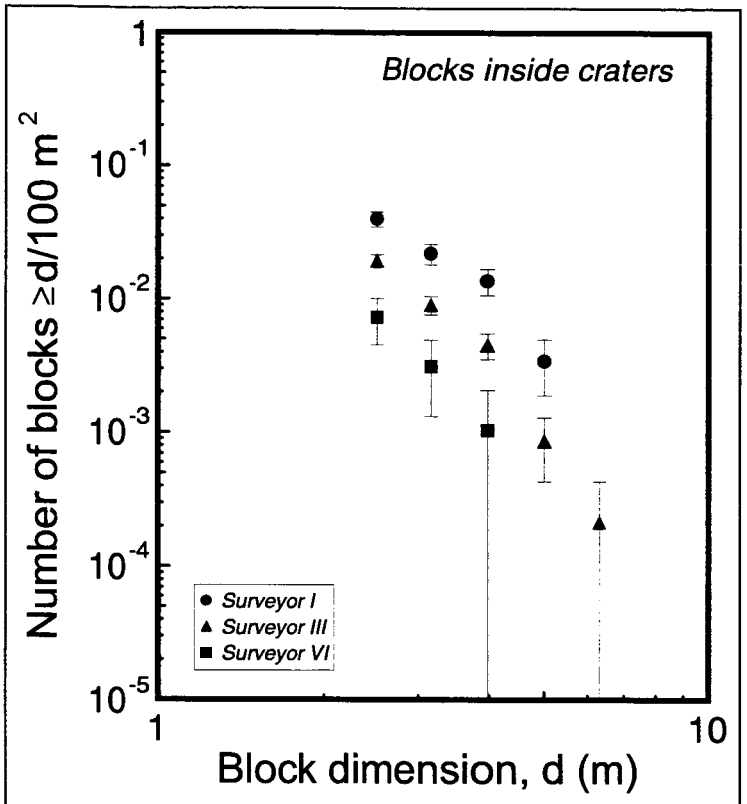

Figure 10. Comparison of the distributions for blocks inside craters at three of the four Surveyor sites studied here.

Intercrater Blocks

The distinction between the three sites in terms of intercrater block density is not as clear as in the previous case (figure 11). In particular, the relative positions of the Surveyor I and Surveyor III sites are reversed, except at the largest sizes. A variety of potential reasons could be suggested but, without supporting data, each would be *ad hoc* in nature and would not materially aid the interpretation of the results. Nevertheless, it is apparent that the shape and position of the Surveyor I distribution in figure 9 is strongly influenced by the density of blocks inside craters at that site.

Discussion

Statistical comparisons—The small number of data points in each distribution unfortunately impairs the interpretive power of formal, statistical comparisons. It is perhaps easiest to judge the similarity or difference between two of the distributions by comparing the actual trends and confidence intervals in the figures given above.

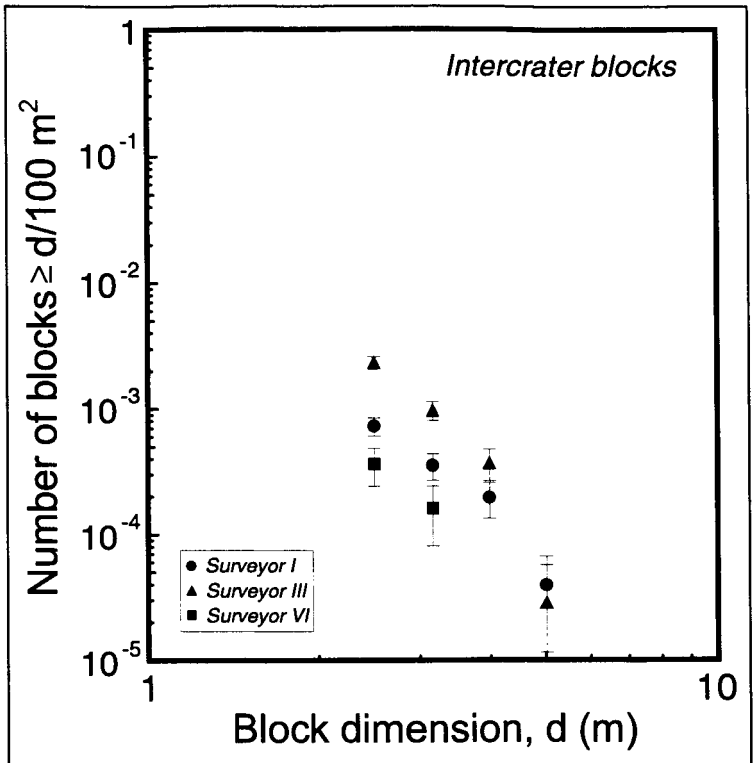

Figure 11. Areal density of intercrater blocks as a function of block dimension at three of the four Surveyor sites studied here.

Another potential means of comparison, given the sparse data, lies in nonparametric methods. The results, however, can vary widely between different types of nonparametric tests and can lead to conflicting interpretations; therefore, it is often recommended that different tests be conducted on the same data. As the interest in these comparisons might be limited, they are presented in Appendix C.

Effects of Regolith Thickness—Some insight into the reasons for the relative positions of the three distributions in figure 10 can be found by examining the block densities in concert with the regolith thicknesses at those sites. A variety of factors are involved in the formation of blocks in the lunar regolith. Each impact that occurs contributes to the evolution of the lunar debris layer, but only those large enough to penetrate the regolith existing at the time will affect the underlying bedrock. An impact forming a crater barely large enough to intersect the bedrock will eject relatively little mass in the form of large blocks, but a substantial volume of blocky material could be created essentially in place, remaining in the crater interior. Somewhat larger craters would possess correspondingly more blocks in their ejecta deposits, while maintaining, or more likely, increasing the interior block population. This trend would continue, perhaps being interrupted by an encounter with a paleoregolith layer below the basalt. Most maria are composed of numerous basalt flows, which occurred over a large span of time (e.g., Boyce, 1975). In many cases an impact-generated regolith was formed in the time between flows, leading to an intercalation of regolith and more coherent basalts.

Clearly, a thicker regolith will require a larger crater to form blocks—interior or exterior—from the underlying, relatively coherent bedrock. Thus, it might be expected that a thin regolith would possess more craters with associated blocks because smaller craters would accomplish the block-forming task, and smaller impacts are considerably more frequent than larger ones (e.g., Öpik, 1960). At the same time, however, blocks

exposed to space would be eroded by even smaller impacts. Thus, a highly interrelated process of block generation and destruction is at work on the Moon, one that is dependent on many factors (e.g., Gault et al., 1972). The simplest picture of block formation, then, maintains that the thinnest regoliths should be accompanied by the highest block densities at the surface since more craters would have penetrated to the bedrock. Indeed, it is difficult to imagine a situation in which this would not be true.

A practical consideration in this study, however, is the limiting resolution of the orbital photography. While a very thin regolith might well be characterized by abundant blocks, only those blocks above the detection limit of the photographic system would be visible. The size of the largest block associated with a crater is directly proportional to the size of that crater (Moore, 1971), so the craters large enough to penetrate a thick regolith will typically possess larger blocks in general. Thus, although thin regoliths might be relatively more blocky than their thicker counterparts, many of those blocks would be below the limit of resolution of existing orbital photography.

An estimate of a regolith's thickness can be made at a given locale on the basis of the morphologies of fresh craters formed in (and through) that regolith (Oberbeck and Quaide, 1967, 1968; Quaide and Oberbeck, 1968). Such estimates for the Surveyor I and III sites exist (Oberbeck and Quaide, 1968), and a similar estimate has been made for a location in Sinus Medii very near the Surveyor VI location (Oberbeck and Quaide, 1968). Telescopic spectral-reflectance data (Pieters, 1978) and photogeologic estimates of surface ages (Boyce et al., 1975) indicate that the measured location in Sinus Medii and the Surveyor VI site are probably on the same basalt unit. As estimated by these methods, median regolith thicknesses at the Surveyor I, III, and VI locations are 3.3, 4.6, and 7.7 m, respectively (Oberbeck and Quaide, 1968). (The concept of regolith thickness at the Surveyor VII site is problematic in that there is no real bedrock stratum relative to which the depth of the debris layer could be measured. Because this location is on the ejecta deposit of a very large crater, it is probable that fragmental ejecta is hundreds of meters thick. Furthermore, these materials were deposited on highland crust, which itself was already severely fragmented by more than four billion years of bombardment.)

It is well known that the largest fragments formed during an impact event occur inside or very near the rim crest of the resulting crater (e.g., Moore, 1971; Öpik, 1971). Thus, the subgroup of blocks within 1.1 radii of crater centers as classified in this study should be useful in examining this modest model. A plot of the cumulative frequencies of blocks against these median regolith thicknesses illustrates that a clear relationship exists between regolith thickness and block density within 1.1 radii of crater centers, at least at these three sites (figure 12). At all sizes measured here, the density of blocks within 1.1 radii of the larger craters is greater at the site with the thinner regolith (Surveyor I), and least at the one with the thickest (Surveyor VI). Thus, as a working hypothesis, it is assumed that block density inside and near the larger craters is inversely proportional to the thickness of the regolith.

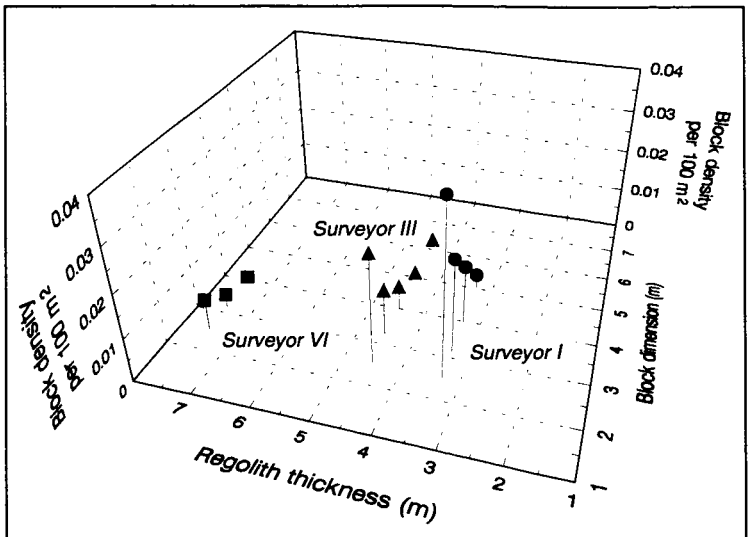

Figure 12. Cumulative block densities inside craters (number of blocks larger than or equal to upper block dimension of each size bin, as in the previous six figures) as a function of block size, plotted relative to the regolith thickness at each site as estimated from crater morphology (Oberbeck and Quaide, 1968). Note the consistently higher densities as thinner regoliths are considered. All axes are cartesian.

A more exhaustive study of this relationship would include a greater number of locales and emphasize the size distribution of craters in each measured area. A single fresh crater, for example, could skew the results considerably by displaying a high density of associated blocks.

COMPARISONS WITH SURVEYOR DATA

Among the products of the extensive set of investigations performed with data obtained by the Surveyor landers are the size and spatial distributions of fragments around the five lander locations. Measurements obtained from Surveyor photography of the lunar surface have been summarized by Shoemaker and Morris (1968), and are used here for comparison with the distributions derived from Lunar Orbiter photography. (The values used here were measured from the graphical data presented by Shoemaker and Morris [1968].) The largest fragments in the Surveyor data set, however, are below a meter in size, so comparisons with the distributions derived here from the orbital photography must be made through extrapolation. Indeed, questions as to the validity of such an extrapolation provided the motivation for much of this study.

Table 3. Least-squares parameters for fits applied to fragment-size distributions as obtained from Surveyor photography by Shoemaker and Morris (1968). Each of these fits is a power-law in form: $\delta=ad^{b}$, where δ is the areal density of fragments equal to or larger than d (per 100 m^2) and d is the fragment size (in meters).

	a	Standard Error	b	Standard Error	r^2
Surveyor I	0.797	+0.409 -0.270	-1.779	0.103	0.900
Surveyor III	0.049	+0.031 -0.019	-2.559	0.111	0.974
Surveyor VI	0.154	-0.056 +0.088	-2.286	0.094	0.983
Surveyor VII	2.666	-0.679 +0.912	-1.802	0.068	0.970

Least-squares fits in the form of power-law relationships were passed through the numerical data derived from the figures presented by (Shoemaker and Morris, 1968). The relevant parameters for these fits are given in table 3. The ideal situation from a hazard analysis point of view would permit the direct extrapolation along such a straight line in log-log space to determine the areal density of fragments of any size. In this way, only a limited amount of data would be required to provide a good estimation of the potential hazard presented by blocks. Unfortunately, this does not appear to be the case in general.

Similar regression analyses were performed on the distributions derived from the orbital photography (table 4), although the utility of these fits is somewhat questionable. The confidence envelopes accompanying these regressions are considerably looser than those for the Surveyor data for two reasons. First, the number of data points and the size range that they cover are much smaller in the case of the large blocks. Second, it is probable that linear fits are inappropriate for the distributions of large blocks. The Surveyor VII site is the exception to these cases because it has a relatively large number of points and appears to follow a linear trend. In all instances, however, the distributions of the larger blocks are substantially steeper than those of the smaller fragments.

Table 4. Least-squares fit parameters for the block distributions derived from the Lunar Orbiter photography. As in the case of the Surveyor-derived data, these are power-law fits. As only two points were available for a point-slope fit, there are no errors provided for the Surveyor VI intercrater subset.

		All blocks		***Inside craters***		***Intercrater***	
		Value	Standard Error	Value	Standard Error	Value	Standard Error
Surveyor I	Coefficient	0.050	+0.039 -0.022	0.889	+0.663 -0.380	0.030	+0.026 -0.014
	Slope	-3.505	±0.468	-3.286	±0.454	-3.931	±0.509
Surveyor III	Coefficient	1.154	+1.647 -0.678	2.454	+2.669 -1.278	0.960	+3.856 -0.769
	Slope	-5.653	±0.625	-4.930	±0.519	-6.159	±1.248
Surveyor III	Coefficient	0.192	+0.793 - 0.154	0.371	+0.165 -0.114	0.009	— —
	Slope	-6.021	±1.403	-4.225	±0.315	-3.522	—
Surveyor III	Coefficient	18.261	+11.109 -6.907	n/a	n/a n/a	n/a	n/a n/a
	Slope	-4.031	±0.141	n/a	n/a	n/a	n/a

An overview of the relationships between the Surveyor and Lunar Orbiter data is given by figure 13. Whether linear fits to the orbital data are appropriate or not, it is apparent that extrapolation of the Surveyor distribution overestimates the areal densities of large blocks in all but the case of the Surveyor III site. The distributions of intercrater blocks, blocks inside craters, and the sum of both fall for the most part inside the 95% confidence envelope around the fit to the Surveyor III data. The envelope around the fit to the Surveyor VI data includes part of the distribution inside craters at that site, but intercrater blocks are well below the extrapolated trend, as is the sum of all blocks. The case for Surveyor I is very similar to that for Surveyor VI.

The shapes of the large block distributions warrant comment. Each of the Surveyor I, II, and VI subsets exhibits a decreasing negative slope with diminishing block size. (The only exception to this observation is the intercrater subset for Surveyor VI, which is represented by only two points.) Figures 5 through 8 illustrate that the loss of blocks due to resolution limitations occurs at substantially smaller sizes than those shown in figure 13. (See also figure 14.) The appearance of this change in slope in the large-block samples at three of the four sites implies that the effect is a real one, and that the steeper (negative) slopes for the larger blocks reflect the lack of fragments in the largest size intervals.

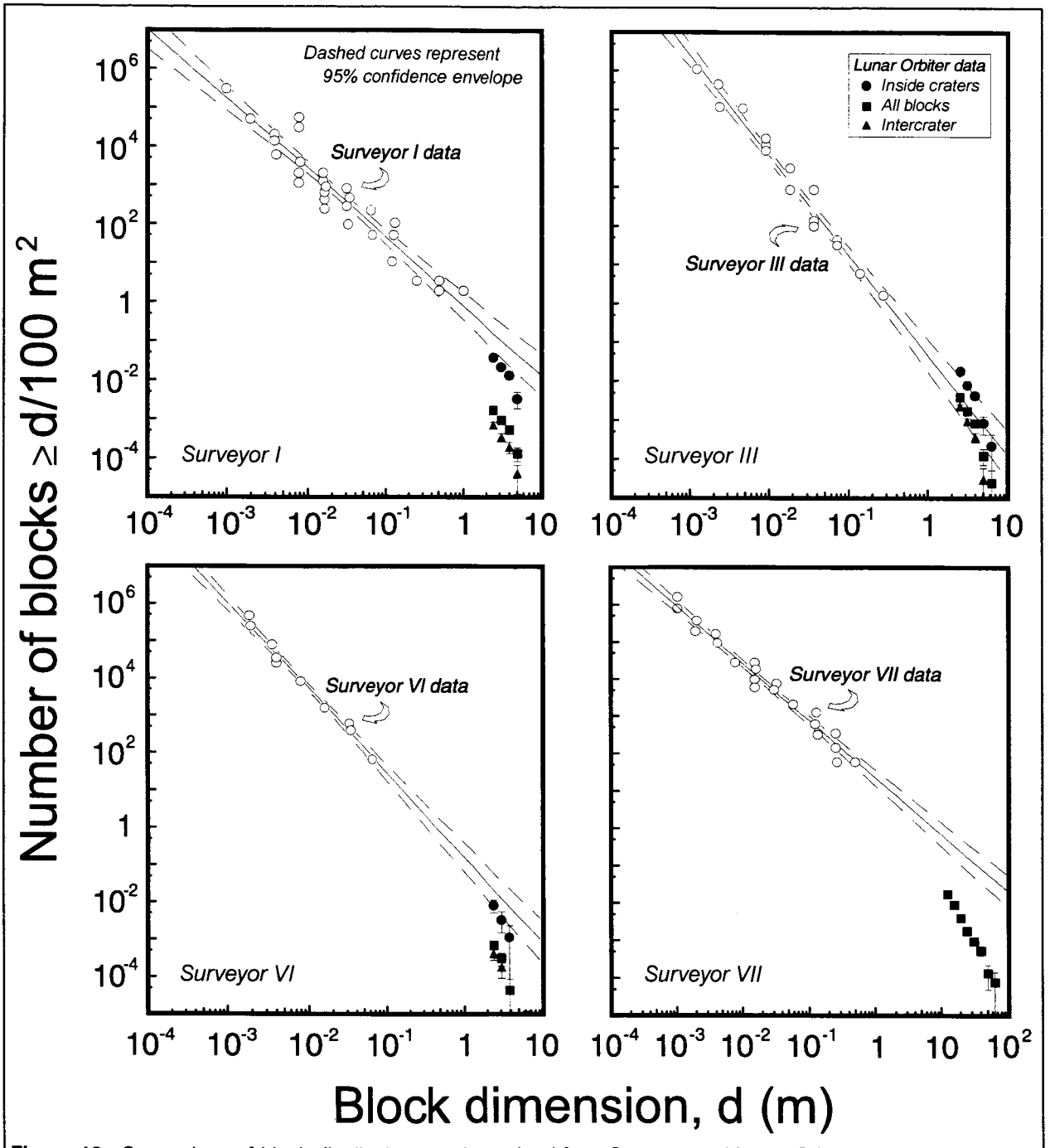

Figure 13. Comparison of block distributions as determined from Surveyor and Lunar Orbiter photography. Only those blocks greater than the line-pair limit of their respective Lunar Orbiter photograph are displayed here.

While the fact that few blocks exist in the largest size intervals might account for the shapes of the distributions, it cannot explain their positions relative to the extrapolated Surveyor trends. Only the Surveyor III site shows reasonable agreement between the orbital and surface-derived data, although as indicated above the slopes are different. The Surveyor I and VI trends are only close to the distributions of blocks inside craters. In both cases, the distributions of all blocks and the intercrater subsets are well below

the extrapolated Surveyor trends. The areal densities of large blocks at the Surveyor VII site also would be overestimated with the Surveyor data. This figure emphasizes the need for additional data to determine the areal density of blocks in the critical range of about 0.5 to 2 m for the mare sites and in the range of 1 to 10 m for the Surveyor VII site. In the absence of new information, the reality of, or reasons for, the differences described above are uncertain.

Blocks in the Immediate Vicinities of the Surveyor Spacecraft

Because the locations of the four Surveyor spacecraft used in this study have been determined with high precision (Whitaker, 1969), it is possible to derive, within the limitations of the data collected from the orbital photography, the distributions of large blocks around the spacecraft. Blocks within 250 m of Surveyor I and Surveyor VI were used as samples for comparison with the data collected from photographs taken by those spacecraft. Surveyor III landed inside a moderately degraded crater; only blocks within that crater were used for comparison with that spacecraft's data set. The photographic coverage of the Surveyor VII site from orbit, while good, was at substantially lower resolution than that for the other three sites. For this reason, reasonably good statistics could be obtained only when blocks within larger areas around the spacecraft were used. Blocks within 1 km and 2 km of the Surveyor VII site were included in two separate comparisons.

The results of these measurements are illustrated in figure 14. Note that, in general, the distributions of large blocks near all four of the Surveyor spacecraft reflect the overall trends shown in figure 13. The extrapolated trend of the Surveyor-based data approaches the densities of the largest size-intervals for the case of the Surveyor I site. An equivalent extrapolation is somewhat closer in the Surveyor III case. The areal density of large blocks immediately around the Surveyor VI spacecraft, however, is almost two orders of magnitude below the extrapolation of the Surveyor VI-based data. Similarly, the distributions derived here for areas within 1 and 2 km of Surveyor VII are below the extrapolated Surveyor data by a substantial degree.

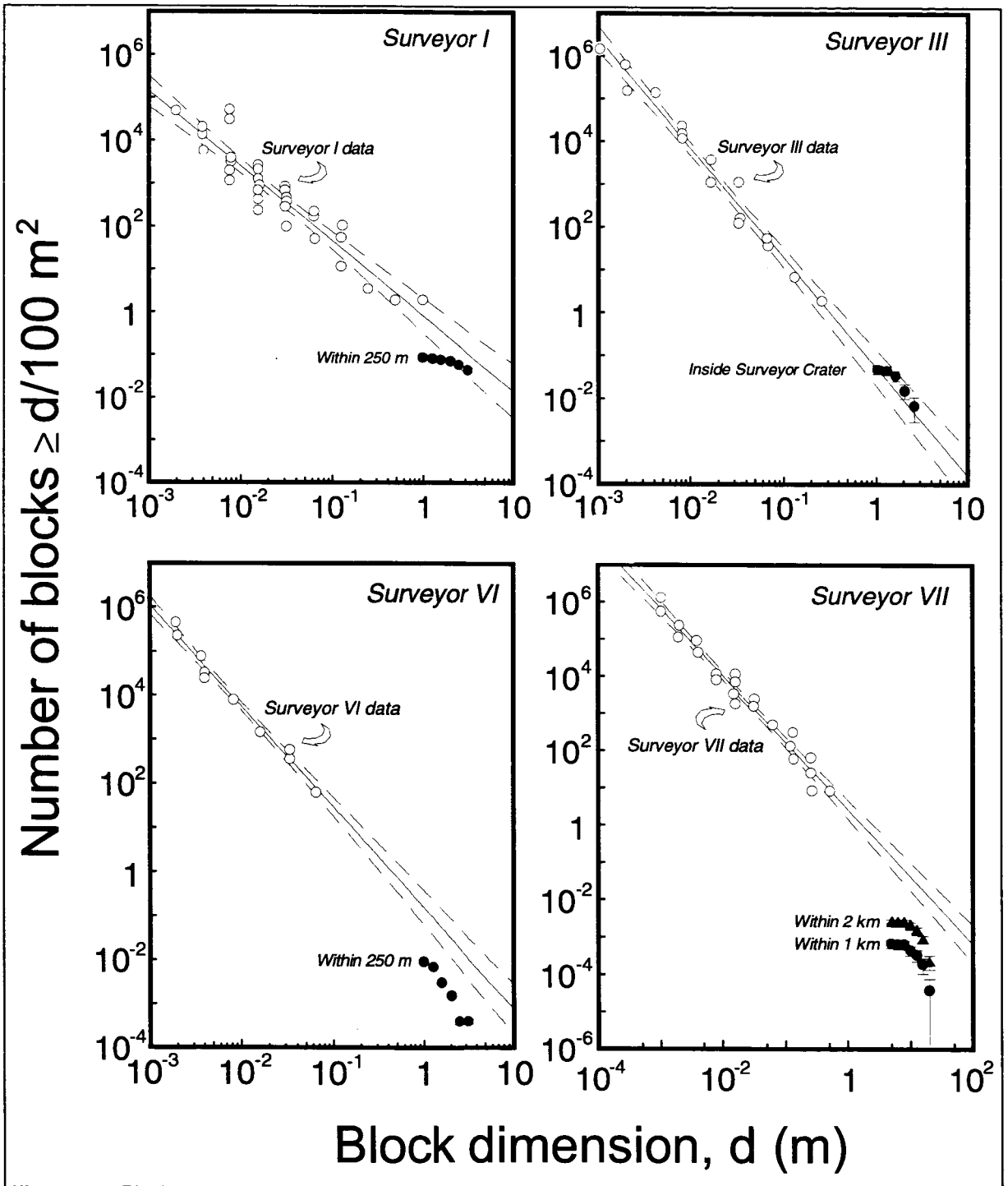

Figure 14. Block distributions in the immediate vicinities of the Surveyor spacecraft. The distributions for the smaller fragments as determined from Surveyor photography are compared to the distributions for larger blocks as measured on Lunar Orbiter photographs. Note the tendency of the extrapolated Surveyor trends to overestimate the densities of larger blocks. Counts for large blocks with sizes equal to the theoretical limit of resolution are presented here to illustrate the point at which photographic limitations affect the shapes of the distributions. Note the different scales for the Surveyor VII pane.

CONCLUSIONS, QUESTIONS, AND RECOMMENDATIONS

Conclusions

The data presented in this report illustrate that self-consistent distributions of large blocks on the lunar surface can be obtained from orbital photography of sufficiently high resolution. This consistency is demonstrated by the similarity in behavior between the subsets of data at the Surveyor I, III, and VI sites, and by the good agreement in position (if not slopes) between the data obtained from Surveyor III photography and those derived from the Lunar Orbiter photographs. (The Surveyor III site is particularly suitable for this purpose in that the blocks measured on both the Surveyor and Lunar Orbiter photography are confined to a well-defined crater.) Confidence in the results is also justified by the well-behaved distribution of large blocks at the Surveyor VII site. The degree of image enlargement relative to the photograph's limiting resolution at this site was similar to those for the other three Surveyor localities, and the quality of illumination for such a study was nearly optimal in all cases. Given these facts and the fact that identical measurement procedures were followed for each location, the distributions obtained for the Surveyor I, III, and VI sites should also be faithful reflections of the block populations in those areas.

Subdivision of the data into block distributions inside craters and in intercrater areas was possible at the three mare sites. The nature of the Surveyor VII site, which possesses few craters of appreciable size, prevented such a distinction. In all three cases, the areal density of blocks within 1.1 radii of craters was about a factor of ten higher than the density in intercrater areas.

Fragment-size distributions have been derived from Surveyor photography taken from the lunar surface (Shoemaker and Morris, 1968). Comparisons between the Surveyor distributions and those derived here from orbital photography permit the following observations: (1) in all cases but Surveyor III, the areal density of large blocks is overestimated by extrapolation of the Surveyor-derived trends, (2) the slopes of the Surveyor-derived distributions are consistently lower than those determined for the large blocks, although statistical uncertainties in the fits to the Surveyor data might permit higher slopes, and thus closer agreement between the two sets of data, and (3) these apparent disagreements could be mitigated if the overall shapes of the cumulative lunar block populations were nonlinear. The relatively large gaps between the Surveyor- and Orbiter-derived data sets, however, do not permit a determination of those shapes.

Questions

Some of the observations made in the course of compiling this report have prompted questions, the more important of which are summarized here.

(1) Although there appears to be a direct relationship between the density of blocks inside craters and the local regolith thickness (figure 11), the relationship between intercrater blocks and regolith thickness is much less clear. Why do the intercrater block densities at the Surveyor I, III, and VI sites appear to be unrelated to the local regolith thickness or at least related in a more complex manner?

(2) What are the limitations of the Surveyor-derived block measurements? Figures 13 and 14 demonstrate that, in some cases, differences between the Surveyor- and Lunar Orbiter-derived block densities span more than an order of magnitude. Insofar as the Surveyor spacecraft did not possess stereo-imaging capability, it is important to know the potential for error in the measurements, as a relatively large moment exists in the fits as extrapolated to the dimensions of the large blocks. The Surveyors, for example, could view the blocks from only one direction. While the same is the case for the orbiters, they could view the blocks in plan, with a substantially better chance of detecting the major axis of a given block. (It is unlikely that the major axis of a block would be oriented normal to the lunar surface.)

(3) What causes the differences in slope between the distributions derived from Surveyor and Lunar Orbiter photography? Are these discrepancies artifacts of the two different methods of data collection, or do they represent a distribution whose shape is size dependent? If the former, which is better for estimating the areal densities of large blocks? It is relevant to note that typical complications associated with measurements near the limits of photographic resolution would yield trends contrary to those measured in this study. In particular, smaller blocks would be lost and underrepresented in the distribution, while larger blocks would be more visible and thus better represented. The result would be trends with shallower slopes than the block populations would actually possess. The fact that each distribution determined from the orbital photography possesses a slope greater than that of the corresponding Surveyor-derived distribution means that either (a) resolution limitations did indeed decrease the slopes, in which case the actual distributions of large blocks are even steeper than pictured in the figures above, or (b) the data used in constructing

the distributions for the large blocks did not suffer from resolution effects and reflect the actual areal densities at these sizes.

Recommendations

Blocks can be hazards to landing spacecraft and more than a simple nuisance to surface vehicles. Mission planning for lunar landing and surface operations will require knowledge of the hazards posed by block populations, among other things, and collection of that information by precursor missions will be an important part of the effort. Doing so will necessitate landed or orbital spacecraft—economic considerations will probably demand that a choice be made between the two. Brief arguments in favor of an orbiter will be summarized here.

The data derived from Lunar Orbiter photography as presented in this report were collected from photographs that are among the best, in terms of resolution, that have been obtained from lunar orbit. Even so, a line-pair limit of about half a meter probably would have permitted a determination of the actual shape of the block distributions at the Surveyor sites across almost four continuous orders of magnitude. Nevertheless, *the data obtained from the Lunar Orbiter photographs yielded distributions limited more by the infrequency of large blocks than by the quality of the photography.* A line-pair limit of less than half a meter would, for all practical purposes, be overkill in terms of hazard detection, provided one-meter features represented the lower limit of such hazards. From this point of view alone, use of a lander or rover to collect such data would be unnecessary. When the extent of areal coverage made possible by an orbiter is also considered, the reasons for hazard analysis by means of landed spacecraft become even less tenable. Tracking of spacecraft in lunar orbit is now sufficiently advanced so that the same photographs used to determine the block populations could also be used to generate high quality topographic maps. Incorporation of multispectral filtering would provide the additional dimension of composition and/or mineralogy to support site selection from a nonhazard point of view. Unless there are other reasons for placing landers or rovers on the lunar surface, hazard analysis can be done more completely, efficiently, and at lower cost with a suitably instrumented, orbiting spacecraft.

In the unlikely event that new data are not made available before the next series of lunar landings are attempted, the data presented above support the following straightforward guidelines:

(1) Intercrater block densities are almost an order of magnitude lower, at a minimum, than those inside craters at all three mare sites examined in this study. The chances of spacecraft damage upon landing would

therefore decrease accordingly if landing sites were targeted only for intercrater mare areas.

(2) In the worst case, such a degree of targeting would not be possible. The least hazardous target would then be a mare site with a thick regolith. Insofar as the limited data indicate that block densities inside and immediately around craters are inversely related to regolith thickness, a blind lander would stand the best chance of survival at such a site. It must be noted, however, that all five Surveyor and three sample return Luna spacecraft successfully performed blind landings.

REFERENCES

Arvidson R.E., Drozd R.J., Guinness E.A., Hohenberg C.M., Morgan C.J., Morrison R.H. and Oberbeck V.R. (1976) Cosmic ray exposure ages of Apollo 17 samples and the age of Tycho. *Proc. Lunar Sci. Conf. 7th*, pp 2817-2832.

Boyce J.M., Dial A.L. and Soderblom L.A. (1974) Ages of the lunar nearside light plains and maria. *Proc. Lunar Sci. Conf. 5th*, pp 11-23.

Boyce J.M., Dial A.L. and Soderblom L.A. (1975) A summary of relative ages of lunar nearside and farside plains. *Astrogeology 66*, U.S. Geological Survey, p 26.

Cameron W.S. and Coyle G.J. (1971) An analysis of the distribution of boulders in the vicinity of small lunar craters. *The Moon*, vol. 3, pp 159-188.

Cintala M.J., Garvin J.B. and Wetzel S.J. (1982) The distribution of blocks around a fresh lunar mare crater (Abstract). *Lunar and Planetary Science XIII*, pp 100-101.

Ferguson G.A. (1966) *Statistical Analysis in Psychology and Education.* p 446, McGraw-Hill, New York.

Gault D.E., Hörz and Hartung J.B. (1972) Effects of microcratering on the lunar surface. *Proc. Lunar Sci. Conf. 3rd*, pp 2713-2734.

Grenander S.U., Cintala M.J., Wood C.A., Head J.W. and Mutch T.A. (1976) Craters and basins on Mercury, Mars, and the Moon. pp 33-34, Division, Austin, TX.

Crater Analysis Techniques Working Group (1979) Standard techniques for presentation and analysis of crater size-frequency data. *Icarus,* vol. 37, pp 467-474.

Hodges C.A., Muelhberger W.R. and Ulrich G.E. (1973) Geologic setting of Apollo 16. *Proc. Lunar Sci. Conf. 4th*, pp 1-25.

Hoel P.G. (1971) *Introduction to Mathematical Statistics.* pp 409, Wiley and Sons, New York.

Jaffe L.D. and Steinbacher R.H. (1969) Introduction. In *Surveyor Program Results, NASA SP-184.* pp 1-12, U.S. Government Printing Office, Washington, DC.

Lee S.W., Thomas P. and Veverka J. (1986) Phobos, Deimos, and the Moon: Size and distribution of crater ejecta blocks. *Icarus*, vol. 68, pp 77-86.

Mood A.M. (1950) *Introduction to the Theory of Statistics.* pp 433, McGraw-Hill Book Company, Inc., New York.

Moore H.J. (1971) Large blocks around lunar craters. *Analysis of Apollo 10 Photography and Visual Observations, NASA SP-232,* pp 26-27.

Muehlberger W.R., Batson R.M., Boudette E.L., Duke M.B., Eggleton R.E., Elston D.P., England A.W., Freeman V.L., Hait M.H., Hall T.A., Head J.W., Hodges C.A., Holt H.E., Jackson E.D., Jordan J.A., Larson K.B., Milton D.J., Reed R.S., Rennilson J.J., Schaber G.G., Schafer J.P., Silver L.T., Stuart-Alexander D.E., Sutton R.L., Swann G.A., Tyner R.L., Ulrich G.E., Wilshire H.G., Wolfe E.W. and Young J.W. (1972) Preliminary geologic investigation of the Apollo 16 landing site. *Apollo 16 Prelim. Sci. Report, NASA SP-315,* pp 6-1 - 6-81.

Neukum G. and König B. (1976) Dating of individual lunar craters. *Proc. Lunar Sci. Conf. 7th*, pp 2867-2881.

Oberbeck V.R. and Quaide W.L. (1967) Estimated thickness of a fragmental surface layer of Oceanus Procellarum. *J. Geophys. Res.*, vol. 72, pp 4697-4704.

Oberbeck V.R. and Quaide W.L. (1968) Generic implications of lunar regolith thickness variations. *Icarus* **9**, pp 446-465.

Öpik E.J. (1960) The lunar surface as an impact counter. *Irish J. Astron.*, vol. 120, pp 404-411.

Öpik E.J. (1971) *Cratering and the Moon's surface.* pp 108-337, Academic Press, New York.

Papanastassiou D.A. and Wasserburg G.J. (1971) Lunar chronology and evolution from Rb-Sr studies of Apollo 11 and 12 samples. *Earth Planet. Sci. Lett.,* vol. 11, pp 37-62.

Pieters C.M. (1978) Mare basalt types on the front side of the moon: A summary of spectral reflectance data. *Proc. Lunar Planet. Sci. Conf. 9th*, pp 2825-2849.

Quaide W.L. and Oberbeck V.R. (1968) Thickness determinations of the lunar surface layer from lunar impact craters. *J. Geophys. Res.,* vol. 73, pp 5247-5270.

Shoemaker E.M. and Morris E.C. (1968) Geology 4. Size-frequency distribution of fragmental debris. In *Surveyor Project Final Report -- Part II. Science Results*, pp 86-102, Jet Propulsion Laboratory, Pasadena, CA.

Shoemaker E.M. and Morris E.C. (1970) Physical characteristics of the lunar regolith determined from Surveyor television observations. *Radio Science,* vol. 5, pp 129-155.

Shoemaker E.M., Morris E.C., Batson R.M., Holt H.E., Larson K.B., Montgomery D.R., Rennilson J.J. and Whitaker E.A. (1969) Television Observations from Surveyor. In *Surveyor Project Final Report. Part II. Science Results*, pp 21-136, Jet Propulsion Laboratory, Pasadena, CA.

Statsoft, Inc. (1993) Statistica for Windows. *Release 4.2*

Turner G. (1971) ^{40}Ar-^{39}Ar ages from the lunar maria. *Earth Planet. Sci. Lett.*, vol. 11, pp 169-191.

Ulrich G.E., Moore H.J., Reed R.S., Wolfe E.W. and Larson K.R. (1981) Ejecta distribution model, South Ray Crater. In *Geology of the Apollo 16 Area, Central Lunar Highlands* (eds. G.E. Ulrich, C.A. Hodges and W.R. Muehlberger), pp 160-173, U.S. Government Printing Office, Washington, DC.

Ulrich G.E., Moore H.J., Reed V.S., Wolfe E.W. and Larson K.B. (1975) Distribution of ejecta from South Ray Crater (Abstract). *Lunar Sci. VI*, pp 832-834.

Whitaker E.A. (1969) Television observations from Surveyor. Location of the Surveyor Spacecraft. In *Surveyor Project Final Report. Part II. Science Results*, pp 35-39, Jet Propulsion Laboratory, Pasadena, CA.

APPENDIX A
Locations and Diameters of Craters with Associated Blocks at the Surveyor Sites

(Negative latitudes are south [below the equator]; longitude is measured to the east where the sub-Earth point is at zero longitude.)

Surveyor I

Crater	Diameter (m)	Latitude	Longitude
1	183	-2.641	316.662
2	307	-2.613	316.665
3	72	-2.647	316.636
4	81	-2.661	316.625
5	73	-2.644	316.685
6	59	-2.667	316.661
7	77	-2.661	316.625

Surveyor III

Crater	Diameter (m)	Latitude	Longitude
1	434	-2.986	336.566
2	43	-3.011	336.562
3	44	-3.018	336.555
4	104	-3.022	336.574
5	47	-3.026	336.568
6	68	-3.019	336.591
7	104	-3.029	336.604
8	34	-3.040	336.607
9	67	-3.025	336.634
10	205	-3.010	336.632
11	58	-2.999	336.629
12	32	-2.989	336.648
13	47	-2.965	336.579
14	31	-2.978	336.571
15	236	-2.999	336.592
16	150	-2.997	336.585
17	73	-3.004	336.582
18	428	-2.987	336.577
19	285	-3.009	336.562
20	82	-3.011	336.597
21	78	-2.978	336.572
22*	661	-3.040	336.588

*Crater 22 is a large crater whose center lies off the southern edge of the study area.

Surveyor VI

Crater	Diameter (m)	Latitude	Longitude
1	146	0.452	358.566
2	21	0.447	358.563
3	26	0.450	358.563
4	21	0.446	358.560
5	33	0.444	358.552
6	26	0.438	358.577
7	14	0.441	358.580
8	12	0.442	358.576
9	21	0.435	358.580
10	17	0.434	358.580
11	30	0.428	358.577
12	89	0.420	358.576
13	19	0.422	358.572
14	97	0.424	358.582
15	43	0.426	358.586
16	28	0.439	358.607
17	38	0.454	358.605
18	26	0.458	358.606
19	24	0.454	358.596
20	36	0.454	358.595
21	102	0.460	358.579
22	30	0.450	358.576
23	65	0.469	358.563
24	157	0.460	358.565
25	31	0.449	358.580
26	84	0.432	358.550
27	46	0.428	358.569

Surveyor VII

Lighting conditions at the Surveyor VII site prevented segregation of the block population according to their positions relative to craters.

APPENDIX B
Areal Densities of Lunar Blocks

Surveyor I

Total Area (m^2)	Area of Prominent Craters (m^2)	Intercrater Area (m^2)
5.248×10^6	1.466×10^6	5.102×10^6

All Blocks

Bin Size (m)	Number of Blocks		Lower Limit	Cumulative Number/ 100 m^2	Upper Limit
	Binned	Cumulative			
>1.0-1.3	5	184	3.247×10^{-3}	3.506×10^{-3}	3.764×10^{-3}
>1.3-1.6	12	179	3.156×10^{-3}	3.411×10^{-3}	3.665×10^{-3}
>1.6-2.0	26	167	2.936×10^{-3}	3.182×10^{-3}	3.428×10^{-3}
>2.0-2.5	46	141	2.460×10^{-3}	2.686×10^{-3}	2.913×10^{-3}
>2.5-3.2	45	95	1.624×10^{-3}	1.810×10^{-3}	1.996×10^{-3}
>3.2-4.0	20	50	8.179×10^{-4}	9.527×10^{-4}	1.087×10^{-3}
>4.0-5.0	23	30	4.672×10^{-4}	5.716×10^{-4}	6.760×10^{-4}
>5.0-6.3	7	7	8.296×10^{-5}	1.334×10^{-4}	1.838×10^{-4}

Blocks inside Craters

Bin Size (m)	Number of Blocks		Lower Limit	Cumulative Number/ 100 m^2	Upper Limit
	Binned	Cumulative			
>1.0-1.3	2	105	6.462×10^{-2}	7.161×10^{-2}	7.860×10^{-2}
>1.3-1.6	7	103	6.332×10^{-2}	7.024×10^{-2}	7.717×10^{-2}
>1.6-2.0	13	96	5.879×10^{-2}	6.547×10^{-2}	7.215×10^{-2}
>2.0-2.5	25	83	5.039×10^{-2}	5.660×0^{-2}	6.282×10^{-2}
>2.5-3.2	26	58	3.436×10^{-2}	3.955×10^{-2}	4.475×10^{-2}
>3.2-4.0	12	32	1.797×10^{-2}	2.182×10^{-2}	2.568×10^{-2}
>4.0-5.0	15	20	1.059×10^{-2}	1.364×10^{-2}	1.669×10^{-2}
>5.0-6.3	5	5	1.885×10^{-3}	3.410×10^{-3}	4.935×10^{-3}

Intercrater Blocks

Bin Size (m)	Number of Blocks		Lower Limit	Cumulative Number/ 100 m^2	Upper Limit
	Binned	Cumulative			
>1.0-1.3	3	79	1.374×10^{-3}	1.548×10^{-3}	1.723×10^{-3}
>1.3-1.6	5	76	1.319×10^{-3}	1.490×10^{-3}	1.661×10^{-3}
>1.6-2.0	13	71	1.226×10^{-3}	1.392×10^{-3}	1.557×10^{-3}
>2.0-2.5	21	58	9.876×10^{-4}	1.137×10^{-3}	1.286×10^{-3}
>2.5-3.2	19	37	6.060×10^{-4}	7.252×10^{-4}	8.445×10^{-4}
>3.2-4.0	8	18	2.697×10^{-4}	3.528×10^{-4}	4.360×10^{-4}
>4.0-5.0	8	10	1.340×10^{-4}	1.960×10^{-4}	2.580×10^{-4}
>5.0-6.3	2	2	1.148×10^{-5}	3.920×10^{-5}	6.692×10^{-5}

Surveyor III

Total Area (m^2)	Area of Prominent Craters (m^2)	Intercrater Area (m^2)
3.972×10^6	4.660×10^5	3.506×10^6

All Blocks

Bin Size (m)	Number of Blocks		Lower Limit	Cumulative Number/ 100 m^2	Upper Limit
	Binned	Cumulative			
>1.0-1.3	52	669	1.619×10^{-2}	1.684×10^{-2}	1.749×10^{-2}
>1.3-1.6	117	617	1.491×10^{-2}	1.553×10^{-2}	1.616×10^{-2}
>1.6-2.0	156	500	1.203×10^{-2}	1.259×10^{-2}	1.315×10^{-2}
>2.0-2.5	172	344	8.194×10^{-3}	8.661×10^{-3}	9.128×10^{-3}
>2.5-3.2	96	172	4.000×10^{-3}	4.330×10^{-3}	4.660×10^{-3}
>3.2-4.0	42	76	1.694×10^{-3}	1.913×10^{-3}	2.133×10^{-3}
>4.0-5.0	29	34	7.092×10^{-4}	8.560×10^{-4}	1.003×10^{-3}
>5.0-6.3	4	5	6.959×10^{-5}	1.259×10^{-4}	1.822×10^{-4}
>6.3-7.9	1	1	0	2.518×10^{-5}	5.035×10^{-5}

Blocks Inside Craters

Bin Size (m)	Number of Blocks		Lower Limit	Cumulative Number/ 100 m^2	Upper Limit
	Binned	Cumulative			
>1.0-1.3	33	417	8.511×10^{-2}	8.949×10^{-2}	9.387×10^{-2}
>1.3-1.6	89	384	7.820×10^{-2}	8.241×10^{-2}	8.661×10^{-2}
>1.6-2.0	104	295	5.962×10^{-2}	6.331×10^{-2}	6.700×10^{-2}
>2.0-2.5	101	191	3.802×10^{-2}	4.099×10^{-2}	4.396×10^{-2}
>2.5-3.2	48	90	1.728×10^{-2}	1.931×10^{-2}	2.135×10^{-2}
>3.2-4.0	21	42	7.623×10^{-3}	9.014×10^{-3}	1.040×10^{-2}
>4.0-5.0	17	21	3.523×10^{-3}	4.507×10^{-3}	5.490×10^{-3}
>5.0-6.3	3	4	4.292×10^{-4}	8.584×10^{-4}	1.288×10^{-3}
>6.3-7.9	1	1	0	2.146×10^{-4}	4.292×10^{-4}

Intercrater Blocks

Bin Size (m)	Number of Blocks		Lower Limit	Cumulative Number/ 100 m^2	Upper Limit
	Binned	Cumulative			
>1.0-1.3	19	252	6.735×10^{-3}	7.188×10^{-3}	7.640×10^{-3}
>1.3-1.6	28	233	6.210×10^{-3}	6.646×10^{-3}	7.081×10^{-3}
>1.6-20	52	205	5.439×10^{-3}	5.847×10^{-3}	6.255×10^{-3}
>2.0-2.5	71	153	4.011×10^{-3}	4.364×10^{-3}	4.717×10^{-3}
>2.5-3.2	48	82	2.081×10^{-3}	2.339×10^{-3}	2.597×10^{-3}
>3.2-4.0	21	34	8.034×10^{-4}	9.698×10^{-4}	1.136×10^{-3}
>4.0-5.0	12	13	2.680×10^{-4}	3.708×10^{-4}	4.736×10^{-4}
>5.0-6.3	1	1	0	2.852×10^{-5}	5.704×10^{-5}

Surveyor VI

Total Area (m^2)	Area of Prominent Craters (m^2)	Intercrater Area (m^2)
2.576×10^6	9.649×10^4	2.479×10^6

All Blocks

Bin Size (m)	Number of Blocks		Lower Limit	Cumulative Number/ 100 m^2	Upper Limit
	Binned	Cumulative			
>1.0-1.3	31	185	6.654×10^{-3}	7.182×10^{-3}	7.710×10^{-3}
>1.3-1.6	57	154	5.497×10^{-3}	5.979×10^{-3}	6.460×10^{-3}
>1.6-2.0	43	97	3.383×10^{-3}	3.766×10^{-3}	4.148×10^{-3}
>2.0-2.5	38	54	1.811×10^{-3}	2.096×10^{-3}	2.382×10^{-3}
>2.5-3.2	9	16	4.659×10^{-4}	6.212×10^{-4}	7.764×10^{-4}
>3.2-4.0	6	7	1.690×10^{-4}	2.718×10^{-4}	3.745×10^{-4}
>4.0-5.0	1	1	0	3.882×10^{-5}	7.764×10^{-5}

Blocks Inside Craters

Bin Size (m)	Number of Blocks		Lower Limit	Cumulative Number/ 100 m^2	Upper Limit
	Binned	Cumulative			
>1.0-1.3	15	86	7.952×10^{-2}	8.913×10^{-2}	9.874×10^{-2}
>1.3-1.6	26	71	6.485×10^{-2}	7.358×10^{-2}	8.232×10^{-2}
>1.6-2.0	15	45	3.969×10^{-2}	4.664×10^{-2}	5.359×10^{-2}
>2.0-2.5	23	30	2.542×10^{-2}	3.109×10^{-2}	3.677×10^{-2}
>2.5-3.2	4	7	4.513×10^{-3}	7.255×10^{-3}	9.997×10^{-3}
>3.2-4.0	2	3	1.314×10^{-3}	3.109×10^{-3}	4.904×10^{-3}
>4.0-5.0	1	1	0	1.036×10^{-3}	2.073×10^{-3}

Intercrater Blocks

Bin Size (m)	Number of Blocks		Lower Limit	Cumulative Number/ 100 m^2	Upper Limit
	Binned	Cumulative			
>1.0-1.3	16	99	3.592×10^{-3}	3.993×10^{-3}	4.394×10^{-3}
>1.3-1.6	31	83	2.980×10^{-3}	3.348×10^{-3}	3.715×10^{-3}
>1.6-2.0	28	52	1.806×10^{-3}	2.097×10^{-3}	2.388×10^{-3}
>2.0-2.5	15	24	7.704×10^{-4}	9.680×10^{-4}	1.166×10^{-3}
>2.5-3.2	5	9	2.420×10^{-4}	3.630×10^{-4}	4.840×10^{-4}
>3.2-4.0	4	4	8.067×10^{-5}	1.613×10^{-4}	2.420×10^{-4}

Surveyor VII

Total Area (m^2)	Area of Prominent Craters (m^2)	Intercrater Area (m^2)
1.051×10^8	1.906×10^7	8.607×10^7

All Blocks

Bin Size (m)	Number of Blocks		Lower Limit	Cumulative Number/ 100 m^2	Upper Limit
	Binned	Cumulative			
>5.0-6.3	19	1265	1.169×10^{-3}	1.203×10^{-3}	1.237×10^{-3}
>6.3-7.9	77	1246	1.152×10^{-3}	1.185×10^{-3}	1.219×10^{-3}
>7.9-10.0	205	1169	1.079×10^{-3}	1.112×10^{-3}	1.144×10^{-3}
>10.0-12.6	336	964	8.874×10^{-4}	9.169×10^{-4}	9.465×10^{-4}
>12.6-15.8	340	628	5.735×10^{-4}	5.973×10^{-4}	6.212×10^{-4}
>15.8-20.0	178	288	2.578×10^{-4}	2.739×10^{-4}	2.901×10^{-4}
>20.0-25.1	67	110	9.465×10^{-5}	1.046×10^{-4}	1.146×10^{-4}
>25.1-31.6	24	43	3.466×10^{-5}	4.090×10^{-5}	4.714×10^{-5}
>31.6-39.8	9	19	1.393×10^{-5}	1.807×10^{-5}	2.222×10^{-5}
>39.8-50.1	8	10	6.504×10^{-6}	9.512×10^{-6}	1.252×10^{-5}
>50.1-63.1	1	2	5.572×10^{-7}	1.902×10^{-6}	3.248×10^{-6}
>63.1-79.4	1	1	0	9.512×10^{-7}	1.902×10^{-6}

APPENDIX C.
Nonparametric statistical comparisons between block distributions

Four nonparametric tests (Statsoft, 1993) were conducted for the distributions between which such comparisons are appropriate; those tests include the Wald-Wolfowitz runs test, the Mann-Whitney U test, the median test, and the Kolmogorov-Smirnov two-sample test. Descriptions of these comparisons and the circumstances of their application can be found in texts such as Mood (1950), Ferguson (1966), and Hoel (1971), and will not be described here.

Table C1. Nonparametric statistical comparisons between different block distributions at the three Surveyor sites. Four entries are contained in each cell; each represents the probability, as calculated by that nonparametric test, that the two compared distributions represent the same population of blocks. Starting in the upper left of each cell and reading clockwise, the values were derived from the Wald-Wolfowitz runs test, the Mann-Whitney U test, the median test, and the Kolmogorov-Smirnov two-sample test. Only those data above the line-pair limit in each block distribution were used in these tests. Meaningless comparisons are represented by dashes in cells; "n.s." in the Kolmogorov-Smirnov case denotes that the differences between the distributions are not significant. The overall structure of this table is diagonally symmetric by construction. All tests were conducted with Statistica for Windows (Statsoft, 1991).

		Surveyor I						Surveyor III						Surveyor VI					
		All		Inside craters		Intercrater		All		Inside craters		Intercrater		All		Inside craters		Intercrater	
Surveyor I	All	—	—	0.02	0.02	0.44	0.25	1.00	0.56	—	—	—	—	1.00	0.13	—	—	—	—
		—	—	<0.05	0.00	n.s.	0.16	n.s.	1.0	—	—	—	—	n.s.	0.41	—	—	—	—
	Inside craters	0.02	0.02	—	—	0.02	0.02	—	—	0.44	0.25	—	—	—	—	0.07	0.05	—	—
		<0.05	0.01	—	—	<0.05	0.01	—	—	n.s.	0.16	—	—	—	—	n.s.	0.01	—	—
	Inter-crater	0.44	0.25	0.02	0.02	—	—	—	—	—	—	1.00	0.39	—	—	—	—	0.22	0.44
		n.s.	0.16	<0.05	0.01	—	—	—	—	—	—	n.s.	0.16	—	—	—	—	n.s.	1.00
Surveyor III	All	1.00	0.56	—	—	—	—	—	—	1.00	0.12	0.02	0.56	0.07	0.05	—	—	—	—
		n.s.	1.00	—	—	—	—	—	—	n.s.	0.53	n.s.	1.00	n.s.	0.01	—	—	—	—
	Inside craters	—	—	0.44	0.25	—	—	1.00	0.12	—	—	0.44	0.08	—	—	1.00	0.13	—	—
		—	—	n.s.	0.16	—	—	n.s.	0.53	—	—	n.s.	0.16	—	—	n.s.	0.41	—	—
	Inter-crater	—	—	—	—	1.00	0.39	0.02	0.56	0.44	0.08	—	—	—	—	—	—	0.22	0.12
		—	—	—	—	n.s.	0.16	n.s.	1.00	n.s.	0.16	—	—	—	—	—	—	n.s.	0.05
Surveyor VI	All	1.00	0.13	—	—	—	—	0.07	0.05	—	—	—	—	—	—	0.07	0.05	0.22	0.44
		n.s.	0.41	—	—	—	—	n.s.	0.01	—	—	—	—	—	—	n.s.	0.01	n.s.	1.0
	Inside craters	—	—	0.07	0.05	—	—	—	—	1.00	0.13	—	—	0.07	0.05	—	—	0.22	0.12
		—	—	n.s.	0.01	—	—	—	—	n.s.	0.41	—	—	n.s.	0.01	—	—	n.s.	0.05
	Inter-crater	—	—	—	—	0.22	0.44	—	—	—	—	0.22	0.12	0.22	0.45	0.22	0.12	—	—
		—	—	—	—	n.s.	1.00	—	—	—	—	n.s.	0.05	n.s.	1.00	n.s.	0.05	—	—

The results of these tests are given in table C1. This attempt to present the data in their most compact form results in some redundancy because the table exhibits diagonal symmetry at different scales. As an example, a comparison of the distribution of blocks inside craters at the Surveyor I site with those inside craters at the Surveyor III site can be found by cross-matching those distributions' respective rows or columns. In this particular case, the null hypothesis that both distributions represent the same block population can be accepted at the 44- (Wald-Wolfowitz test), 25- (Mann-Whitney U-test), and 16-percent (median test) confidence levels. The Kolmogorov-Smirnov two-sample

test indicated that there is no significant difference between the two distributions. Comparisons of each distribution with itself are meaningless, and intersite comparisons between the different subsets of blocks were not made.

In standard statistical studies, the null hypothesis typically is accepted if the confidence level is 0.05 or greater (i.e., the distributions are taken to be derived from different populations only if there is a 95 percent or greater probability that this is the case). This is not a strict rule, however, and each application of these data must entail a definition of its own acceptable uncertainties. Inspection of the table shows that, even with the nonparametric tests, results of the comparisons can be ambiguous.

APPENDIX D
Locations of the Surveyor I, III, VI, and VII Spacecraft

Locations of the Surveyor spacecraft in the coordinate system used in this report. Longitude in this case is measured to the east with 0° at the sub-Earth point.

	Latitude	Longitude
Surveyor I	-2.637	316.657
Surveyor III	-2.999	336.586
Surveyor VI	0.436	358.571
Surveyor VII	-41.149	348.563

APPENDIX E
Fragment Size Distributions Derived from Surveyor Photography

The values given in these tables were derived from illustrations presented by Shoemaker et al. (1969). Multiple distributions, each representing a different area near the spacecraft, were presented for each site. Nonuniformity of fragment sizes is due to conversion from graphical data.

Surveyor I

Fragment Size (m)	Cumulative Number/ 100 m^2
0.001	3.236×10^5
0.002	5.370×10^4
0.004	2.188×10^4
0.008	4.266×10^3
0.016	4.365×10^2
0.004	1.445×10^4
0.008	2.089×10^3
0.016	7.079×10^2
0.032	1.000×10^2
0.004	6.166×10^3
0.008	3.388×10^3
0.015	1.349×10^3
0.031	8.913×10^2
0.063	2.291×10^2
0.129	1.122×10^2
0.008	1.230×10^3
0.016	9.120×10^2
0.032	4.786×10^2
0.063	1.778×10^2
0.126	54.95
0.016	2.455×10^2
0.032	97.72
0.065	52.48
0.123	11.75
0.490	1.995
0.977	1.995
0.008	3.236×10^4
0.015	2.188×10^3
0.031	3.020×10^2
0.008	5.495×10^4
0.016	2.818×10^3
0.032	3.890×10^2
0.031	7.244×10^2
0.245	3.631
0.501	3.631

Surveyor III

Fragment Size (m)	Cumulative Number/ 100 m^2
0.001	1.479×10^6
0.002	6.310×10^5
0.004	1.445×10^5
0.008	1.585×10^4
0.002	1.549×10^5
0.008	2.344×10^4
0.016	3.981×10^3
0.032	1.122×10^3
0.008	1.175×10^4
0.016	1.122×10^3
0.033	1.660×10^2
0.064	54.95
0.032	1.230×10^2
0.065	38.02
0.129	7.079
0.251	1.950

Surveyor VI

Fragment Size (m)	Cumulative Number/ 100 m^2
0.002	4.571×10^5
0.004	7.762×10^4
0.033	5.888×10^2
0.002	2.399×10^5
0.004	2.455×10^4
0.008	7.943×10^3
0.032	5.248×10^2
0.004	3.236×10^4
0.008	8.710×10^3
0.016	1.514×10^3
0.034	3.631×10^2
0.065	63.10

Surveyor VII

Fragment Size (m)	Cumulative Number/ 100 m^2
0.001	1.413×10^6
0.002	2.344×10^5
0.004	9.550×10^4
0.008	1.202×10^4
0.015	1.202×10^4
0.001	5.623×10^5
0.002	1.175×10^5
0.004	4.677×10^4
0.016	7.244×10^3
0.004	3.981×10^4
0.008	1.318×10^4
0.032	2.630×10^3
0.129	3.236×10^2
0.251	67.61
0.008	8.511×10^3
0.015	3.548×10^3
0.030	1.585×10^3
0.060	5.370×10^2
0.120	1.380×10^2
0.251	25.12
0.015	1.905×10^3
0.132	64.57
0.263	8.318
0.501	8.318

REPORT DOCUMENTATION PAGE

Form Approved
OMB No. 0704-0188

1. AGENCY USE ONLY (Leave Blank)	2. REPORT DATE	3. REPORT TYPE AND DATES COVERED
	October 1995	NASA Technical Memorandum

4. TITLE AND SUBTITLE

Block Distributions on the Lunar Surface: A Comparison Between Measurements Obtained From Surface and Orbital Photography

5. FUNDING NUMBERS

6. AUTHOR(S)

Mark J. Cintala; Kathleen M. McBride*

7. PERFORMING ORGANIZATION NAME(S) AND ADDRESS(ES)

Lyndon B. Johnson Space Center
Earth Science and Solar System Exploration Division
Houston, Texas 77058

8. PERFORMING ORGANIZATION REPORT NUMBERS

S-782

9. SPONSORING/MONITORING AGENCY NAME(S) AND ADDRESS(ES)

National Aeronautics and Space Administration
Washington, DC 20546-0001

10. SPONSORING/MONITORING AGENCY REPORT NUMBER

TM-104804

11. SUPPLEMENTARY NOTES

*Lockheed Engineering and Science Company, Houston, Texas

12a. DISTRIBUTION/AVAILABILITY STATEMENT

Unclassified/Unlimited
Available from the NASA Center for AeroSpace Information (CASI)
800 Elkridge Landing Road
Linthicum Heights, MD 21090-2934
(301) 621-0390 Subject Category: 91

12b. DISTRIBUTION CODE

13. ABSTRACT *(Maximum 200 words)*

Among the hazards that must be negotiated by lunar-landing spacecraft are blocks on the surface of the Moon. Unfortunately, few data exist that can be used to evaluate the threat posed by such blocks to landing spacecraft. Perhaps the best information is that obtained from Surveyor photographs, but those data do not extend to the dimensions of the large blocks that would pose the greatest hazard. Block distributions in the vicinities of the Surveyor I, III, VI, and VII sites have been determined from Lunar Orbiter photography and are presented here. Only large (i.e., greater than or equal to 2.5 m) blocks are measurable in these pictures, resulting in a size gap between the Surveyor and Lunar Orbiter distributions. Nevertheless, the orbital data are self-consistent, a claim supported by the similarity in behavior between the subsets of data from the Surveyor I, III, and VI sites and by the good agreement in position (if not slopes) between the data obtained from Surveyor III photography and those derived from the Lunar Orbiter photographs. Confidence in the results is also justified by the well-behaved distribution of large blocks at the surveyor site.

Comparisons between the Surveyor distributions and those derived from the orbital photography permit these observations: (1) in all cases but that for Surveyor III, the density of large blocks is overestimated by extrapolation of the Surveyor-derived trends, (2) the slopes of the Surveyor-derived distributions are consistently lower than those determined for the large blocks, and (3) these apparent disagreements could be mitigated if the overall shapes of the cumulative lunar block populations were nonlinear, allowing for different slopes over different size intervals. The relatively large gaps between the surveyor-derived and Orbiter-derived data sets, however, do not permit a determination of those shapes.

14. SUBJECT TERMS

Lunar Landing Sites; Lunar Topography; Lunar Maps; Lunar Photography; Lunar Orbiter; Lunar Probes

15. NUMBER OF PAGES
44

16. PRICE CODE

17. SECURITY CLASSIFICATION OF REPORT	18. SECURITY CLASSIFICATION OF THIS PAGE	19. SECURITY CLASSIFICATION OF ABSTRACT	20. LIMITATION OF ABSTRACT
Unclassified	Unclassified	Unclassified	Unlimited